Imaging the earth's interior using seismic waves: Body waves and surface waves

Barbara ROMANOWICZ

Collège de France and IPG Paris
University of California, Berkeley

VonReubeur Paschwitz
1889

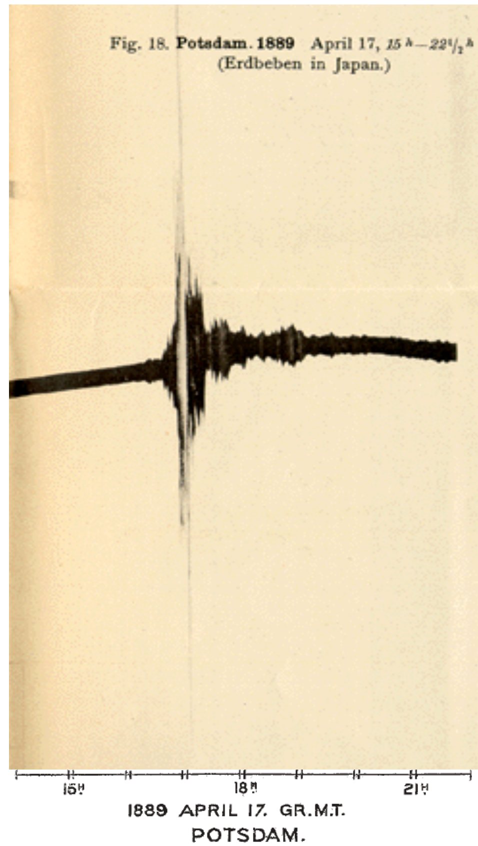

"Reading the report on this earthquake in NATURE (June 13, p. 162), I was struck by its coincidence in time with a very singular perturbation registered by two delicate horizontal pendulums at the Observatories of Potsdam and Wilhelmshaven."
VonRebeur Paschwitz, E., Nature, 40, July 25, 1889

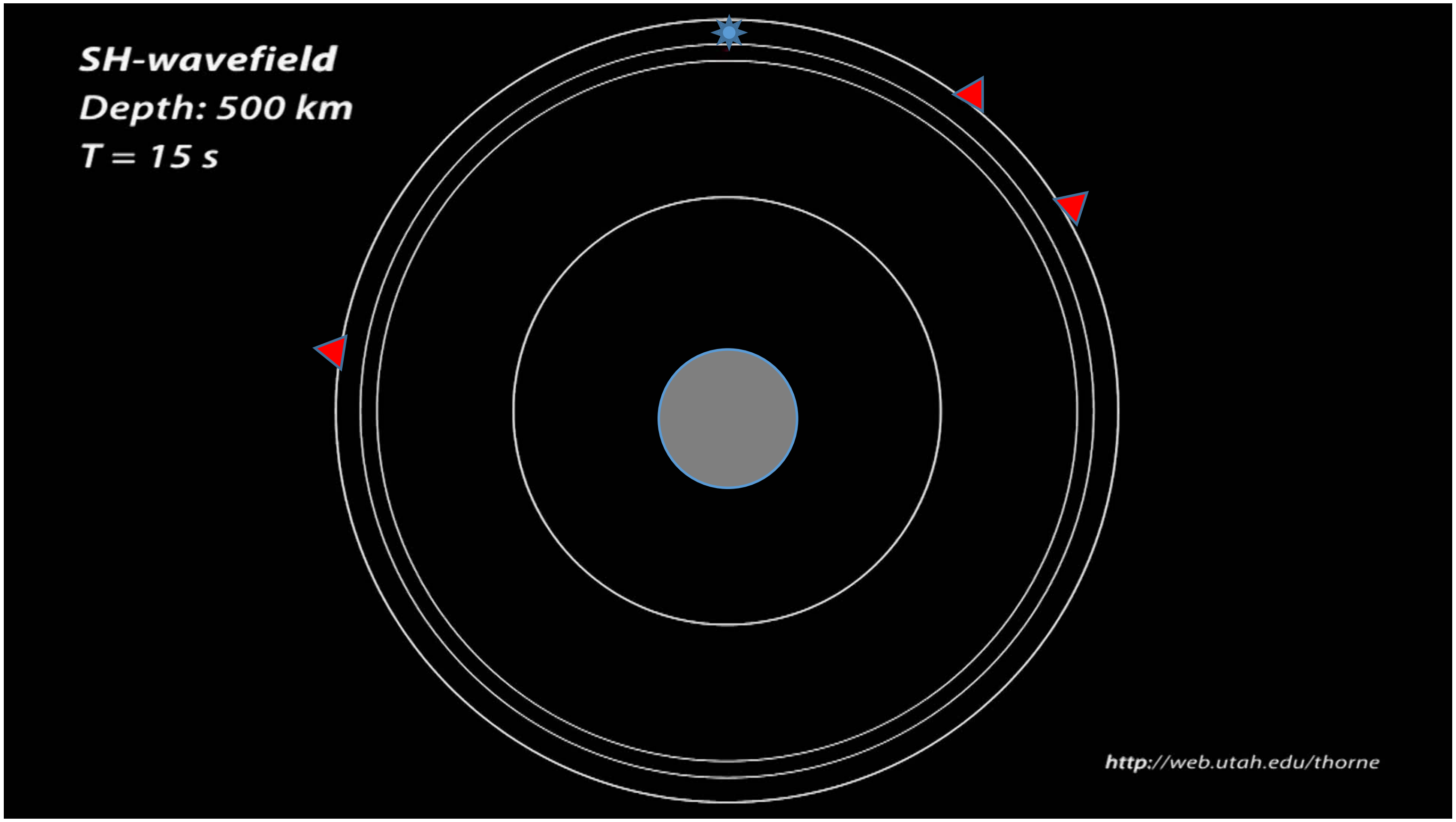
SH-wavefield
Depth: 500 km
T = 15 s
http://web.utah.edu/thorne

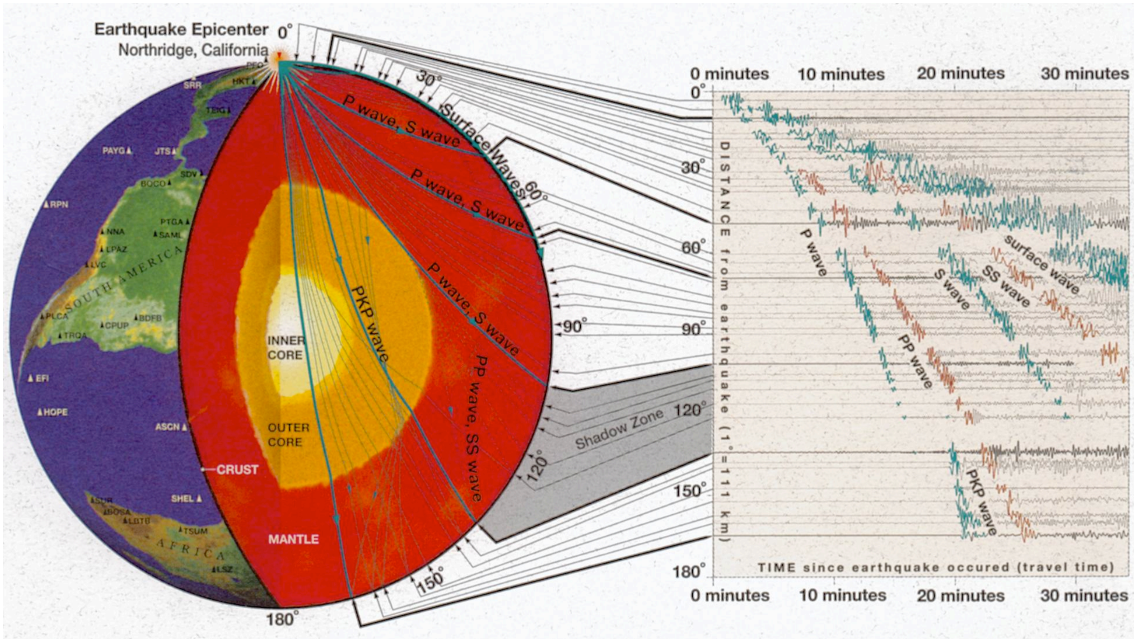

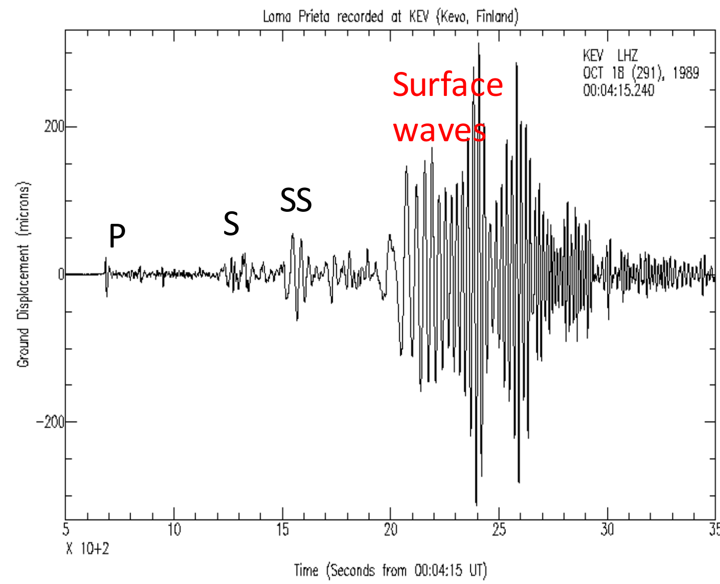

← 50 minutes →

->Seismic waves propagate at different speeds depending on the composition and the temperature of the material they traverse.

->They are refracted and reflected on structural boundaries, such as the core-mantle boundary, the earth's surface, or the upper mantle discontinuities that correspond to mineral phase transitions.

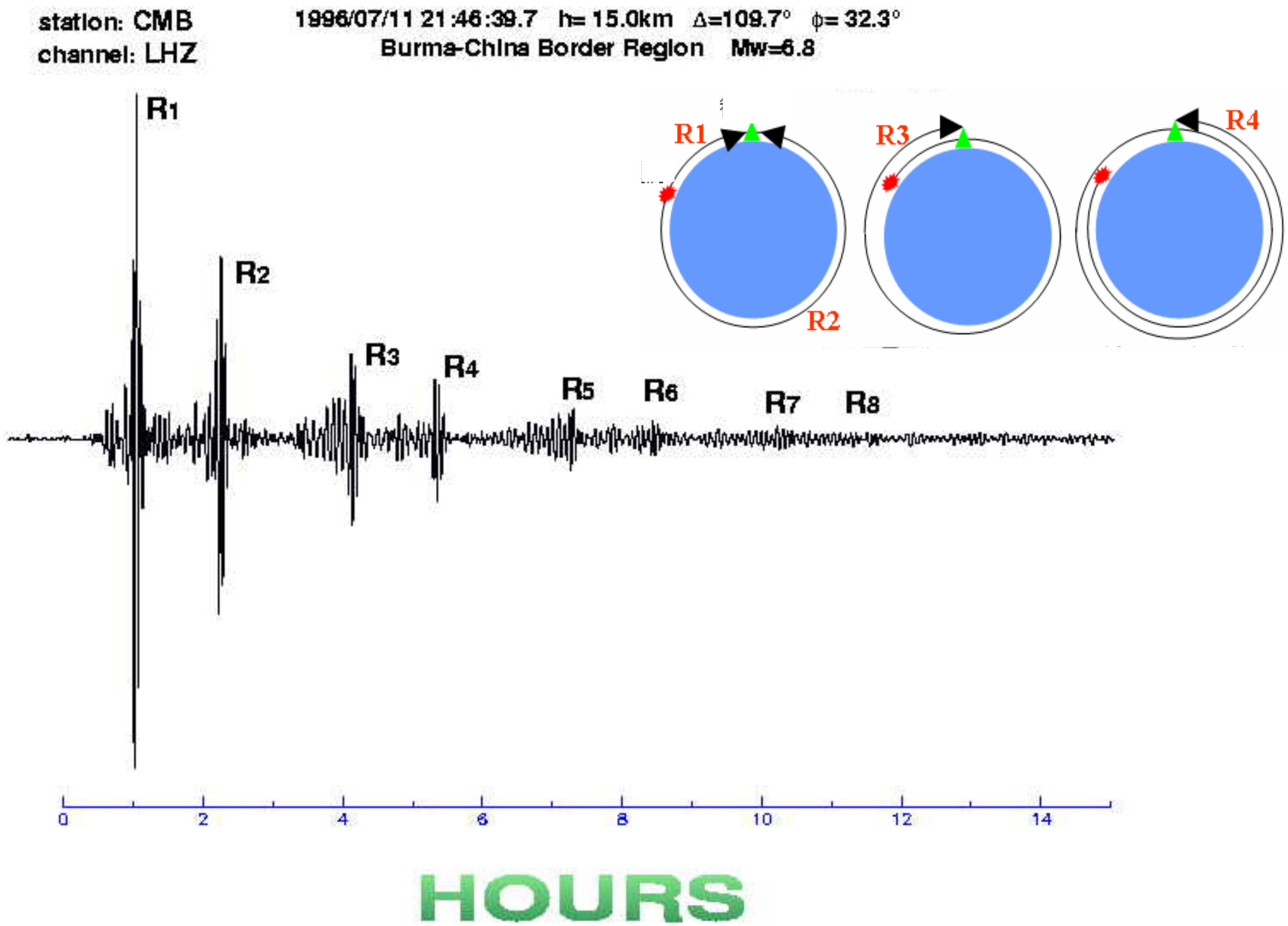
station: CMB
channel: LHZ
1996/07/11 21:46:39.7 h= 15.0km Δ=109.7° ϕ= 32.3°
Burma-China Border Region Mw=6.8
R1
R2
R3
R4
R5
R6
R7
R8
R1
R2
R3
R4
0
2
4
6
8
10
12
14
HOURS

Earth's free oscillations generated by the great Sumatra earthquake of December 26, 2004, M_w 9.2

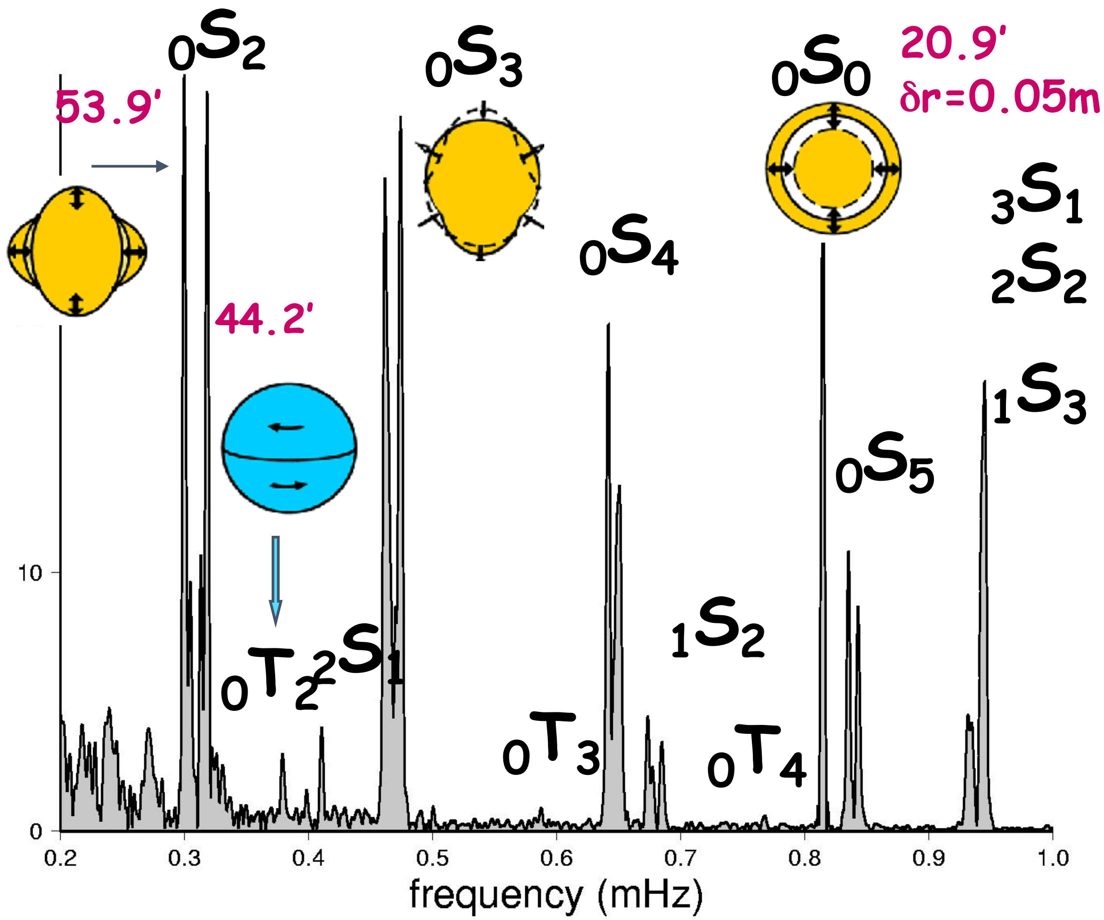

Courtesy of G. Roult

Figure 2.4-7: Seismic spectrum for various studies.

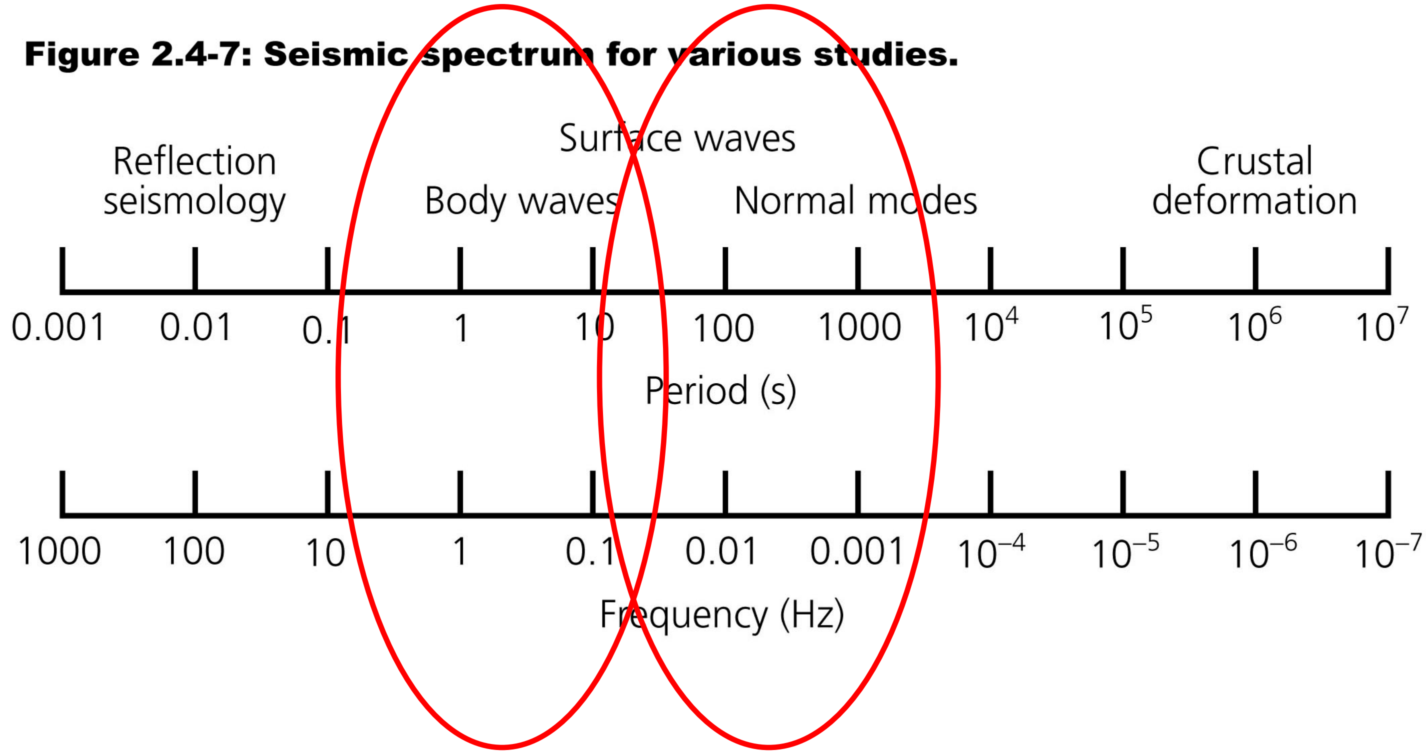

From Stein and Wysession, 2003

displacement

Equation of motion:

$$\rho \frac{\partial^2 u_i}{\partial t^2} = \sigma_{ij,j} + F_i$$ i=1..3 or: $$\rho \ddot{u} = \nabla \cdot \underline{\sigma} + \vec{F}$$

density

stresses

Body forces

Hooke's law (linear elasticity):

$$\sigma_{ij} = c_{ijkl}\varepsilon_{kl}$$

Valid for $\varepsilon < 10^{-4}$

Strains:

$$\varepsilon_{ij} = u_{i,j} + u_{j,i} = \frac{1}{2}\left(\frac{\partial u_i}{\partial x_j} + \frac{\partial u_i}{\partial x_j}\right)$$

C_{ijkl} is the "elastic tensor"

- characteristic of material being deformed
- because of symmetries it has "only" 21 independent elements

Elasticity: Linear stress-strain relationship

$$\sigma_{ij} = c_{ijkl}\varepsilon_{kl}$$

"Hooke's law"
Strains <10^{-4}

Simplest case: isotropic material:

Properties are the same in all directions

There are only 2 independent elastic parameters:

$$\sigma_{ij} = \lambda\delta_{ij}\epsilon_{kk} + 2\mu\epsilon_{ij}$$

$\varepsilon_{kk} = \varepsilon_{11} + \varepsilon_{22} + \varepsilon_{33}$ (dilatation)

Kronecker delta ($\delta_{ij} = 1$ for $i = j$, $\delta_{ij} = 0$ for $i \neq j$)

λ and μ = Lamé parameters

In an isotropic medium, wave speed depends NEITHER on the direction of propagation NOR polarization direction

Isotropic medium representations:

$$\sigma_{ij} = \lambda\delta_{ij}\epsilon_{kk} + 2\mu\epsilon_{ij}$$

An isotropic medium is described by the space distribution of:

(ρ, λ, μ)

or:

(ρ, κ, μ)

or:

(ρ, α, β)

- ρ — Density
- μ — Shear modulus: measure of the resistance of material to shear.
- $\kappa = \lambda + \frac{2}{3}\mu$ — Bulk modulus: measure of incompressibility of a material. Given by hydrostatic stress divided by fractional volume change.
- $\alpha = \sqrt{\dfrac{\lambda + 2\mu}{\rho}}$ — P velocity (velocity of compressional waves)
- $\beta = \sqrt{\dfrac{\mu}{\rho}}$ — S velocity (velocity of shear waves)
- $V_\phi = \sqrt{\dfrac{\kappa}{\rho}}$ — Bulk sound velocity

$\boxed{\text{Equation of motion:}}$

$$\rho \frac{\partial^2 u_i}{\partial t^2} = \sigma_{ij,j} + F_i$$

or:

$$\rho \ddot{u} = \nabla \cdot \underline{\sigma} + \vec{F}$$

stresses

Body forces

Hooke's law (isotropic elastic material):

$$\sigma_{ij} = \lambda \delta_{ij} \varepsilon_{kk} + 2\mu \varepsilon_{ij}$$

Strains:

$$\varepsilon_{ij} = u_{i,j} + u_{j,i} = \frac{1}{2}\left(\frac{\partial u_i}{\partial x_j} + \frac{\partial u_i}{\partial x_j}\right)$$

Seismic wave equation in an isotropic medium:

$$\rho \ddot{\mathbf{u}} = \nabla \lambda (\nabla \cdot \mathbf{u}) + \nabla \mu \cdot [\nabla \mathbf{u} + (\nabla \mathbf{u})^T] + (\lambda + 2\mu) \nabla \nabla \cdot \mathbf{u} - \mu \nabla \times \nabla \times \mathbf{u} + \vec{F}$$

Homogeneous wave equation governs wave propagation outside of source regions (F =0)

$$\rho\ddot{\mathbf{u}} = \cancel{\nabla\lambda}(\nabla\cdot\mathbf{u}) + \cancel{\nabla\mu}\cdot[\nabla\mathbf{u} + (\nabla\mathbf{u})^T] + (\lambda+2\mu)\nabla\nabla\cdot\mathbf{u} - \mu\nabla\times\nabla\times\mathbf{u}$$

In a homogeneous medium (constant λ and μ), the first 2 terms are zero:

$$\rho\ddot{\mathbf{u}} = (\lambda + \cancel{2}\mu)\nabla\nabla\cdot\mathbf{u} - \mu\nabla\times\cancel{\nabla}\times\mathbf{u} \qquad (2)$$

(1) Taking the divergence of equation (2) : Remember: $\nabla\cdot(\nabla\times\mathbf{\Psi}) = 0$

$$\nabla^2(\nabla\cdot\mathbf{u}) - \frac{1}{\alpha^2}\frac{\partial^2(\nabla\cdot\mathbf{u})}{\partial t^2} = 0 \qquad \alpha^2 = \frac{\lambda+2\mu}{\rho}$$

Compressional wave (P-wave) propagating at speed α

(2) Taking the curl of equation (2): Remember: $\nabla\cdot(\nabla\times\mathbf{u}) = 0,$

$\nabla\times(\nabla\phi) = 0$

$$\nabla^2(\nabla\times\mathbf{u}) - \frac{1}{\beta^2}\frac{\partial^2(\nabla\times\mathbf{u})}{\partial t^2} = 0. \qquad \beta^2 = \frac{\mu}{\rho}$$

Shear wave (S-wave) involving no volume change propagating at speed β

Solutions are waves…

u(**x**,*t*)= f(**x**±**v***t*) where v= velocity

In Cartesian coordinates, plane waves:

$$u(\mathbf{x},t) = A\exp(i(\omega t \pm \mathbf{k}\cdot\mathbf{x}))$$

<u>**k**</u> is the wave number: $$\mathbf{v} = \frac{\omega}{\mathbf{k}}$$

In spherical coordinates:

$$u(r,t) = \frac{f(t \pm r/v)}{r}$$

Amplitudes decay as 1/r: geometrical spreading

Figure 2.4-1: Plane wave fronts.

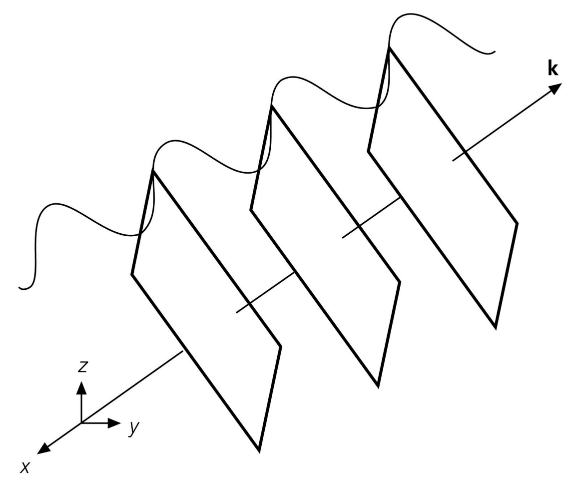

(Figures from Stein and Wysession, 2003)

Figure 2.4-2: Approximation of a spherical wave front as plane waves.

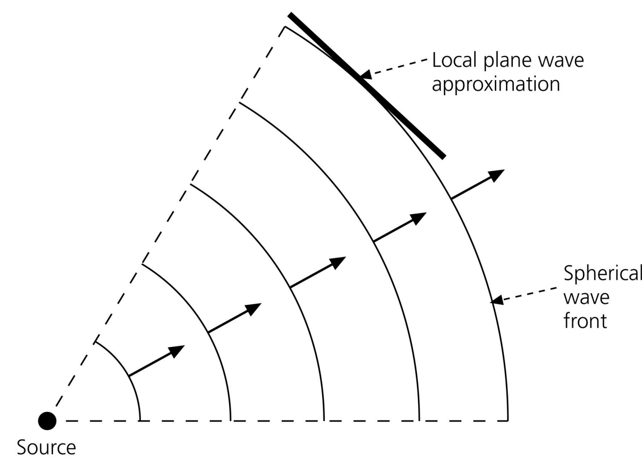

Wavefronts and raypaths

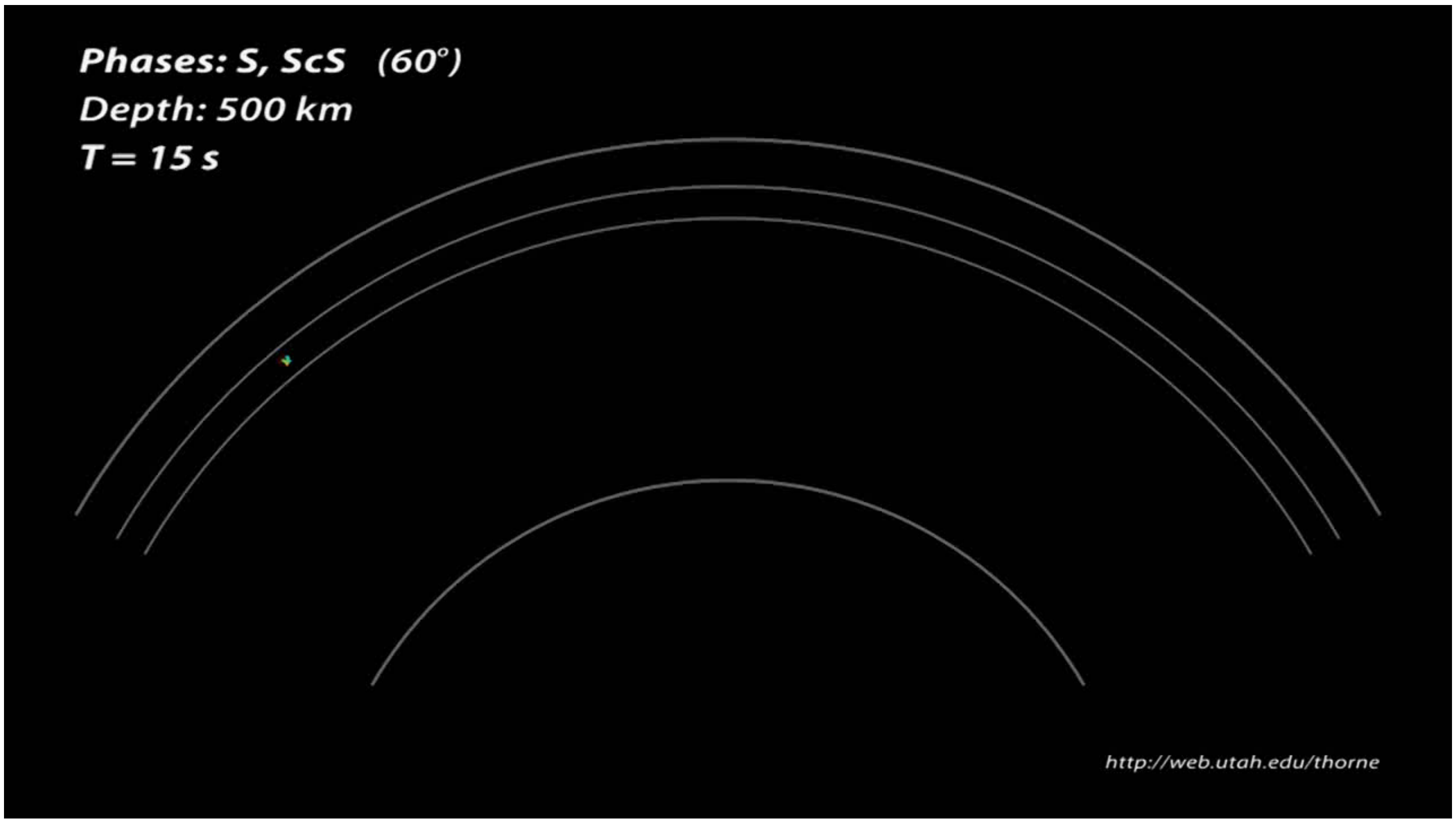

P and S waves

http://www.geo.mtu.edu/UPSeis/images/

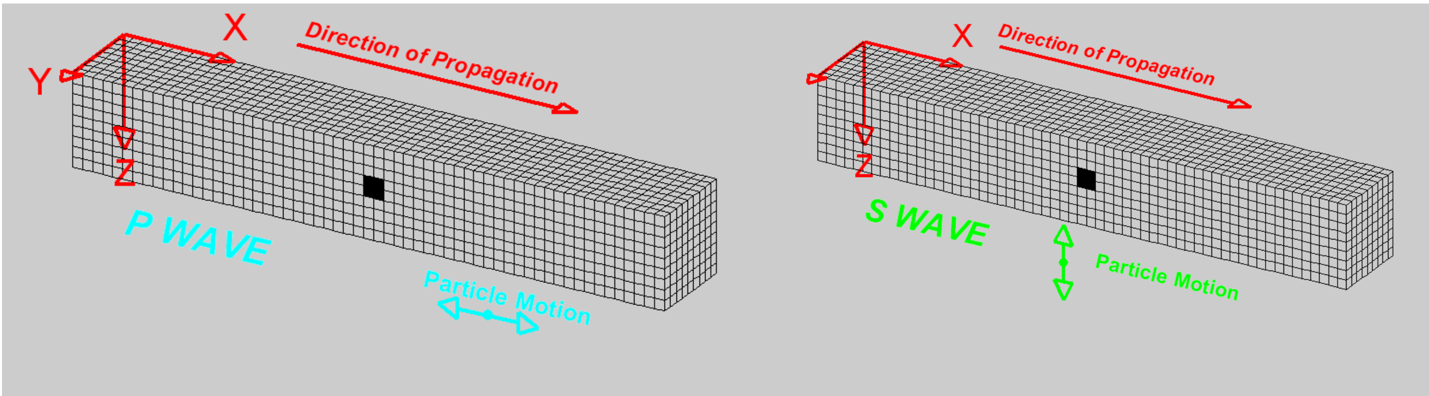

- **P waves**: volume & shape change, particle motion in the direction of propagation
- **S waves**: only shape change (no volume change), particle motion perpendicular to direction of propagation
  - SH – particle motion in the horizontal plane
  - SV – particle motion in the vertical plane

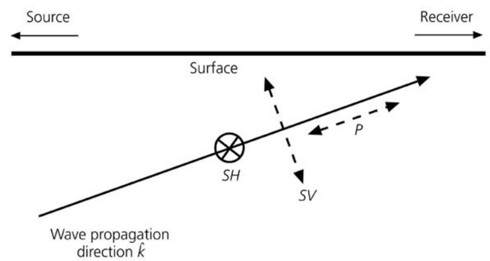

Example: Particle motion plots for SKS+SKKS and Sdiff

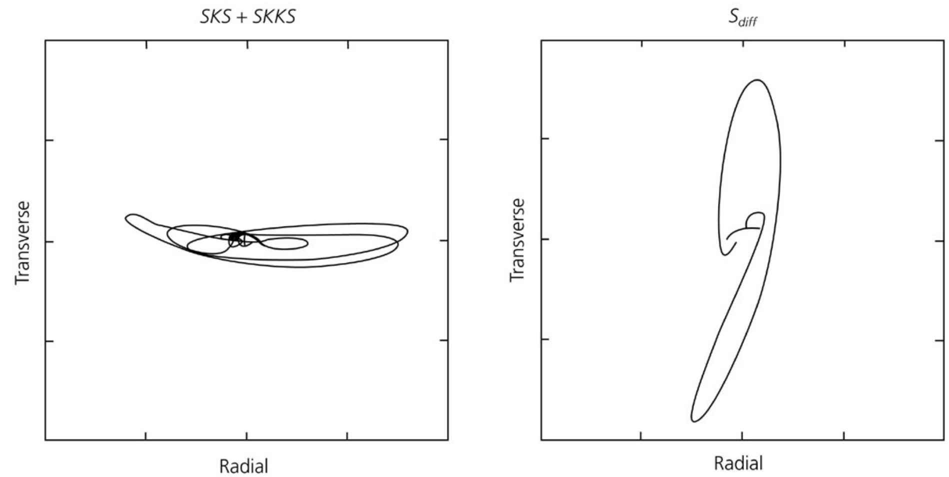

From Stein and Wysession, 2003

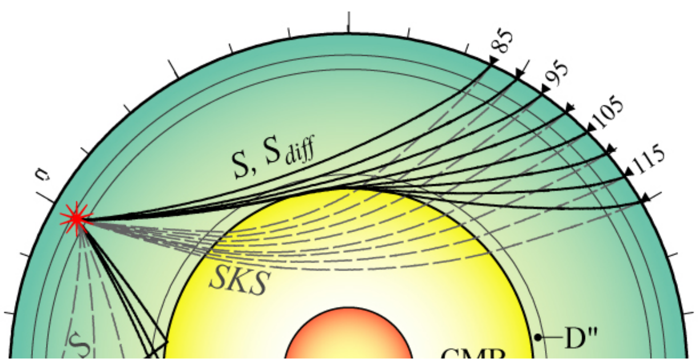

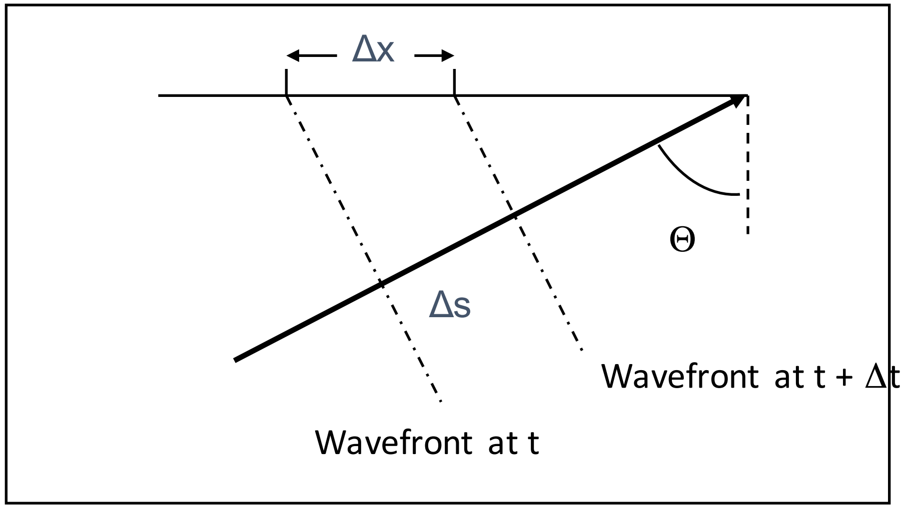

Vertical plane containing the direction of propagation

Define incidence angle θ, then:

$$\Delta s = v\Delta t = \Delta x \cdot \sin\theta$$

v = propagation velocity

u = 1/v = slowness

or:

$$\frac{\Delta t}{\Delta x} = \frac{\sin\theta}{v} = p$$

p "ray parameter" – apparent horizontal slowness

Snell's Law – the ray parameter

For the wavefield to remain continuous along interface between regions with different velocities, waves will change direction in addition to their speed.

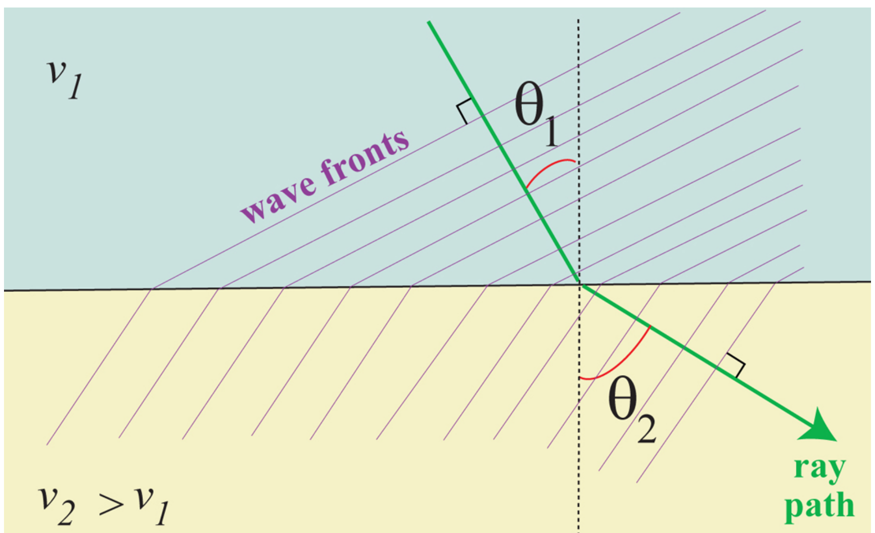

- Snell's Law: $$\frac{\sin\theta_1}{v_1} = \frac{\sin\theta_2}{v_2} = p$$
- Ray parameter (horizontal slowness) remains the same along the ray path

Layered / shell medium

By specifying a ray parameter and a starting location, we fix the ray-path through a layered or spherically-symmetric Earth

The deepest depth the ray can reach is one where:

$$\frac{\Delta t}{\Delta x} = \frac{\sin\theta}{v} = p$$

$$\frac{\sin 90}{v_1} = \frac{1}{v_1} = p$$

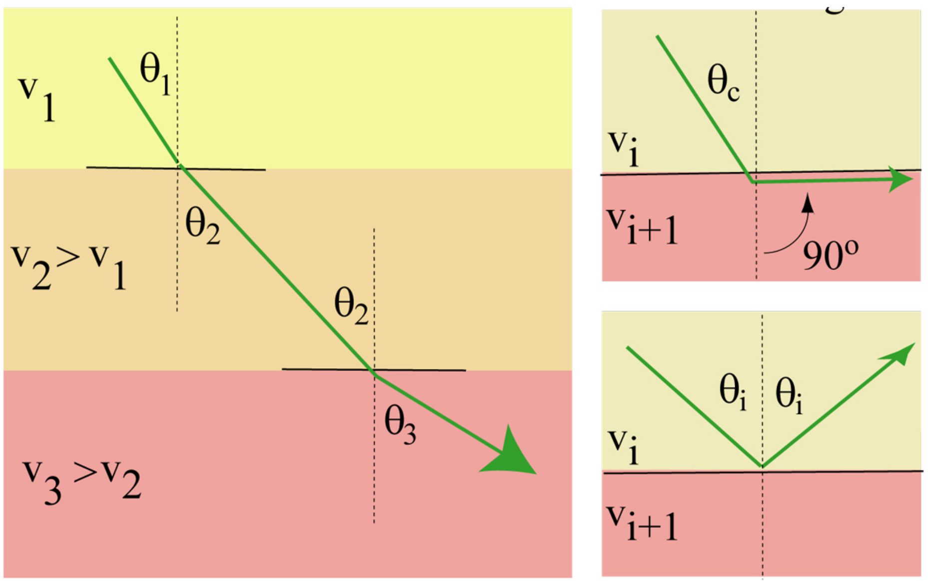

figure from garnero.asu.edu

In general, some of the energy is transmitted, some reflected, and, in the P-SV case, some converted

SH case

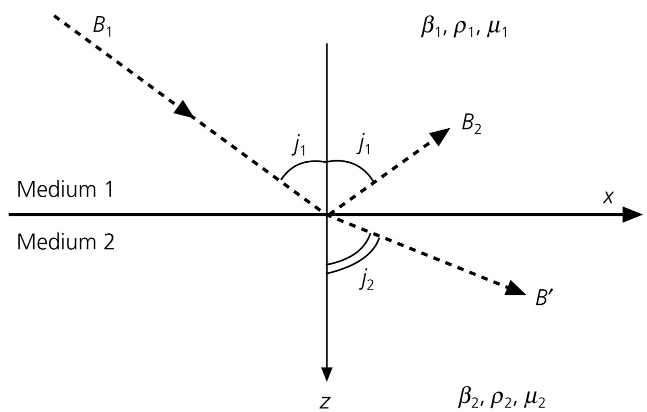

P-SV case

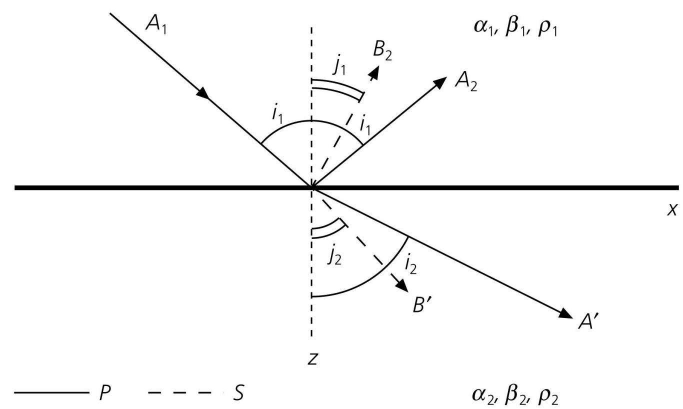

Angles of reflection/transmission depend only on velocities
Amplitudes depend on impedance (ρ v)

Receiver functions

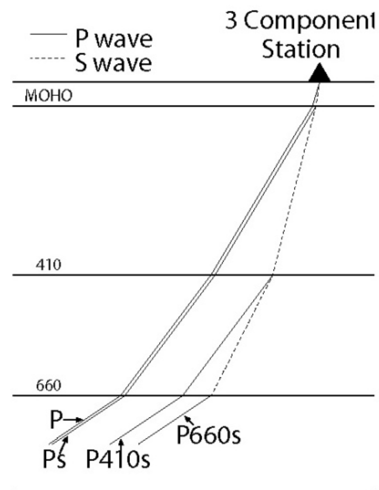

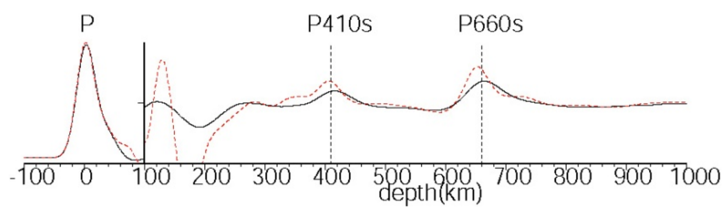

Ray paths in spherical geometry,
when velocity increases with depth

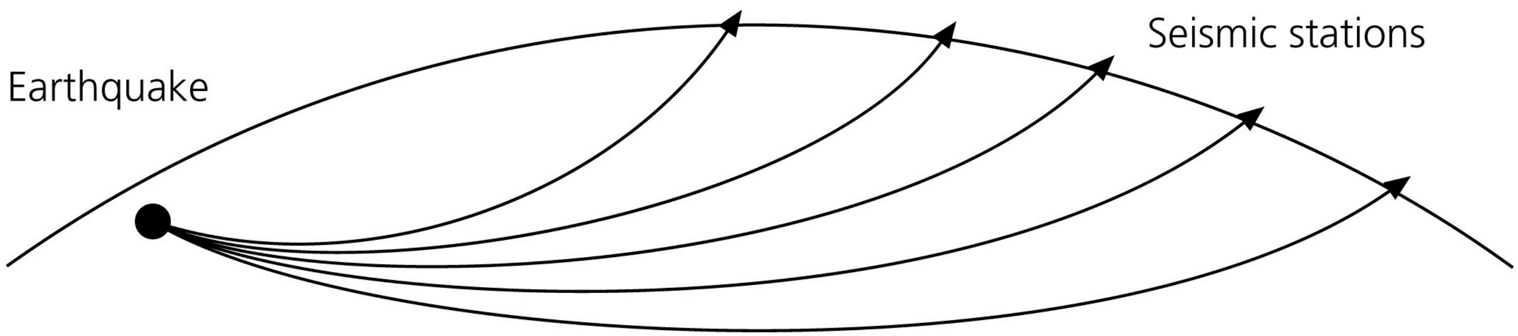

Steep gradients, such as upper-mantle discontinuities,
create triplications

Figure 3.5-12: Ray paths for *P* waves through the upper mantle.

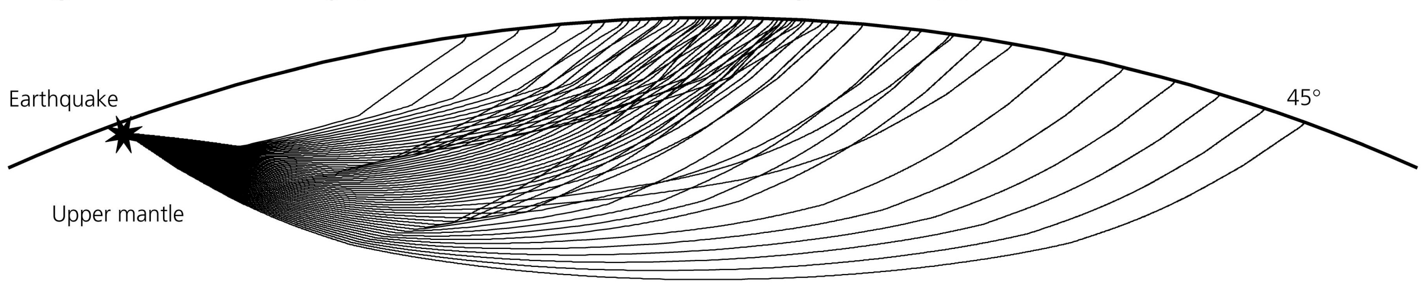

Triplications

figures from Shearer, 2009

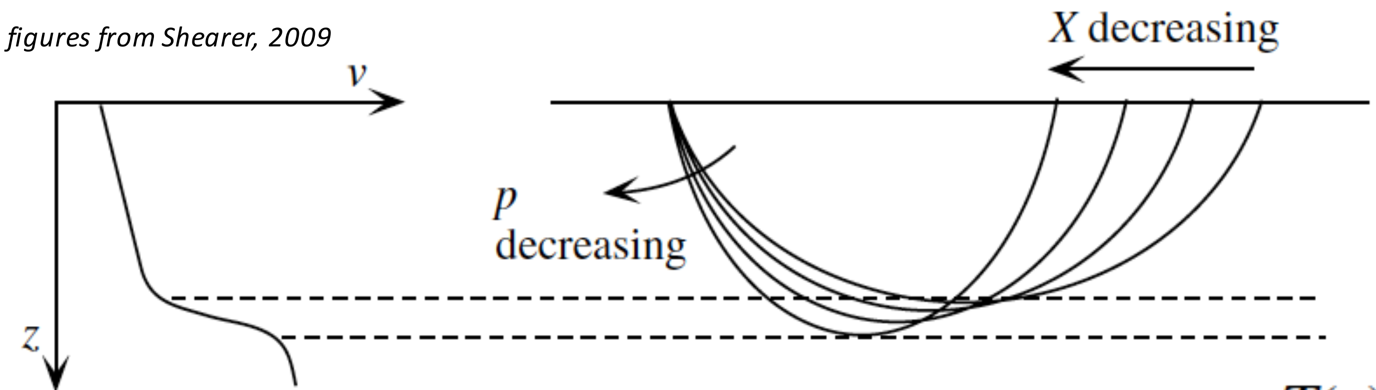

- Depth ranges in which velocity increases rapidly with depth can produce triplications: multiple rays (with different horizontal slownesses) arrive at the same time
- Transition zone discontinuities produce triplications
- At epicentral distances > 30° rays bottom in the lower mantle and no triplications are (typically) observed

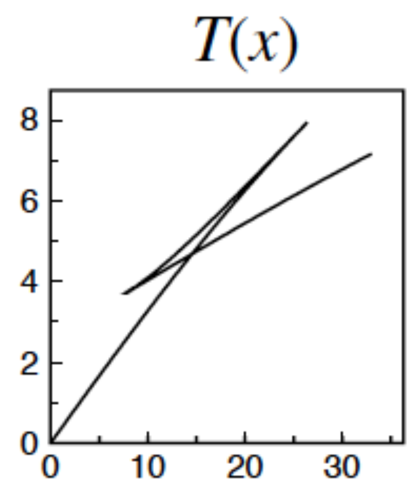

• Shadow zones

Rays cannot bottom in a depth range where velocity decreases with depth*

Low-velocity zones produce shadow zones

Prominent shadow zone in PKP waves due to low velocities in the outer core

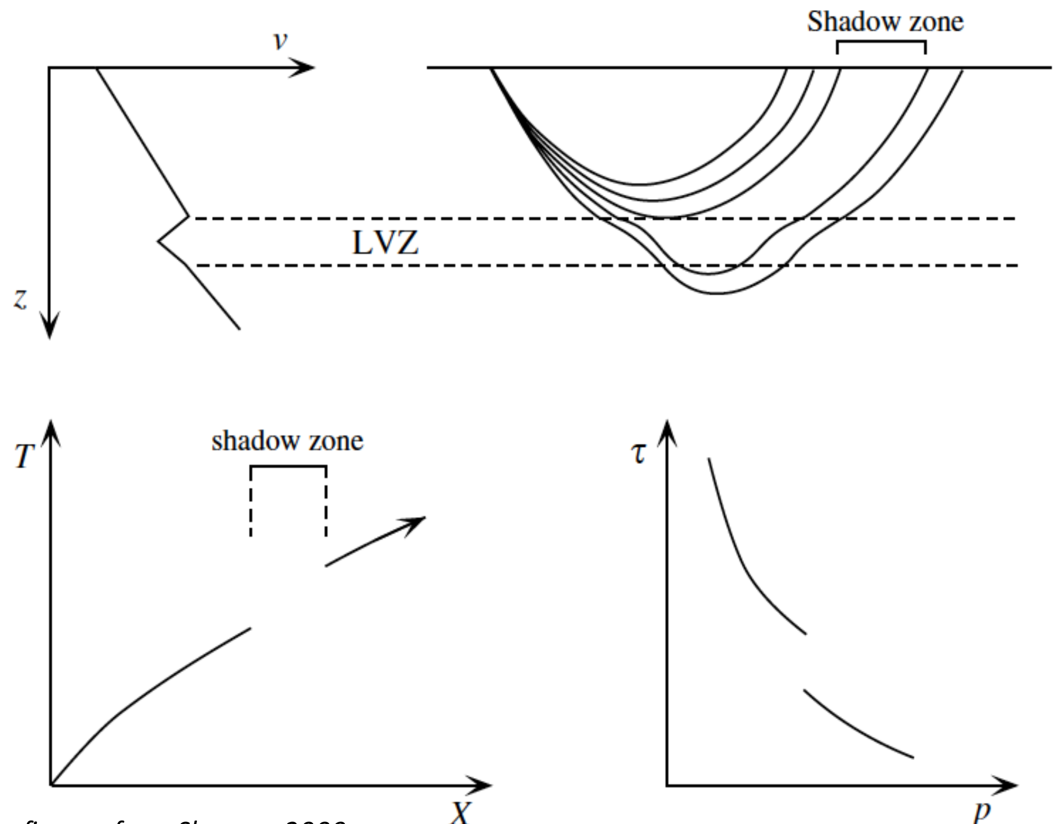

figures from Shearer, 2009

Low velocity layers create shadow zones

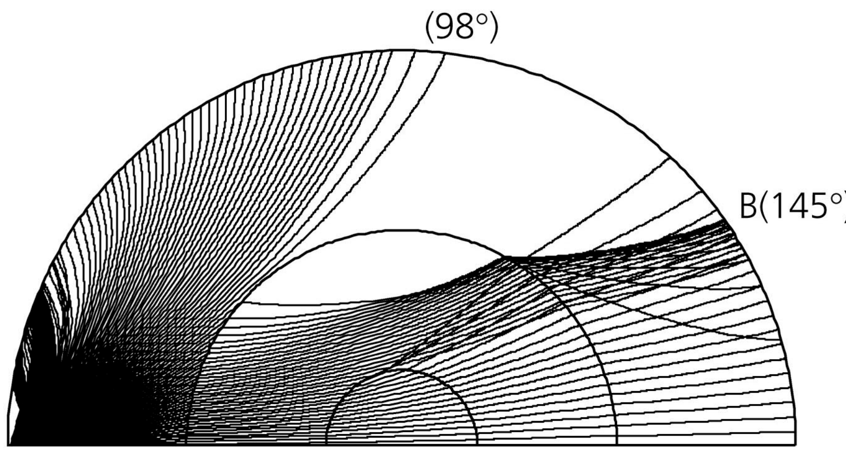

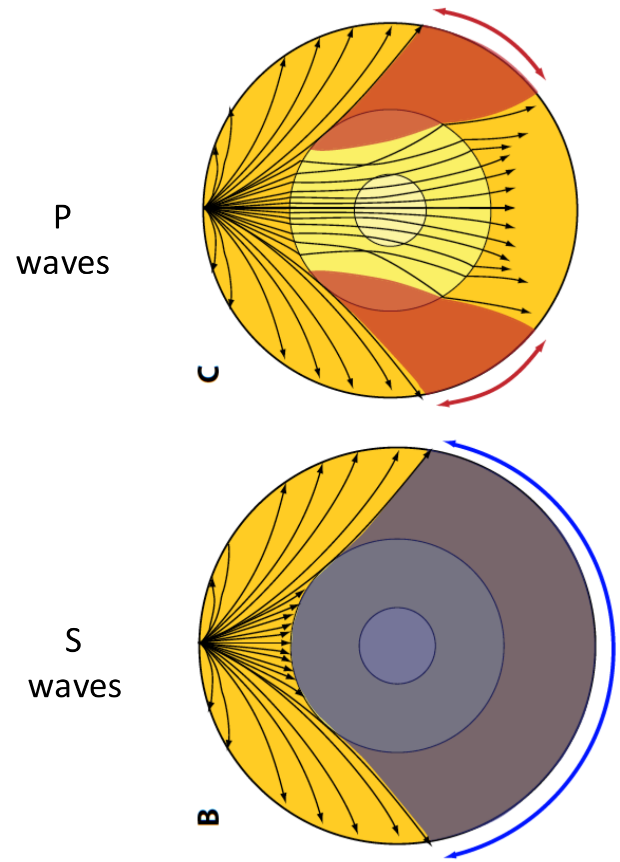

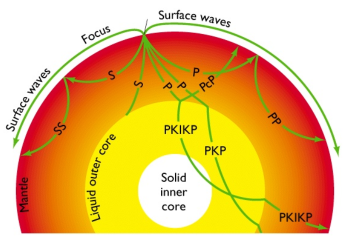

Observed and theoretical travel time curves

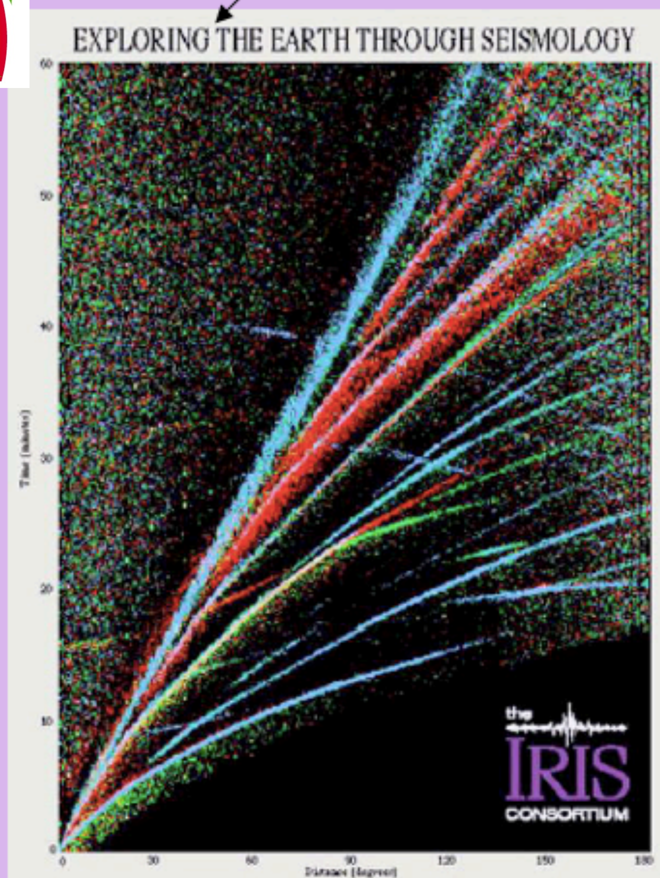

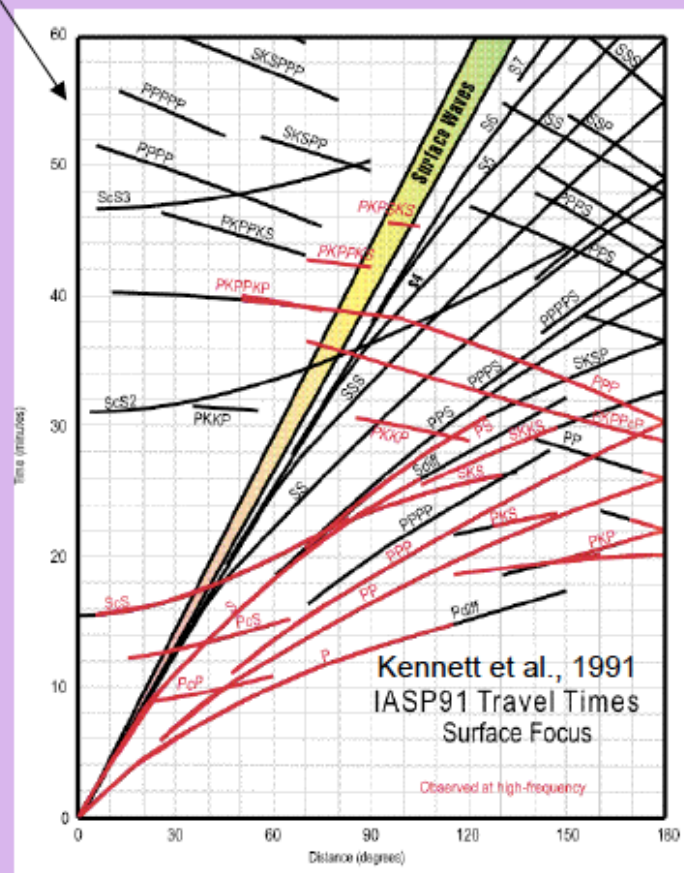

SS and PP precursors (reflection)

- SS (or PP) precursors are waves reflected from a discontinuity in the subsurface and observed before the arrival of the surface-reflected wave
- Their amplitude (as a function of epicentral distance) can constrain both Vp, Vs and density jumps across mantle discontinuities!

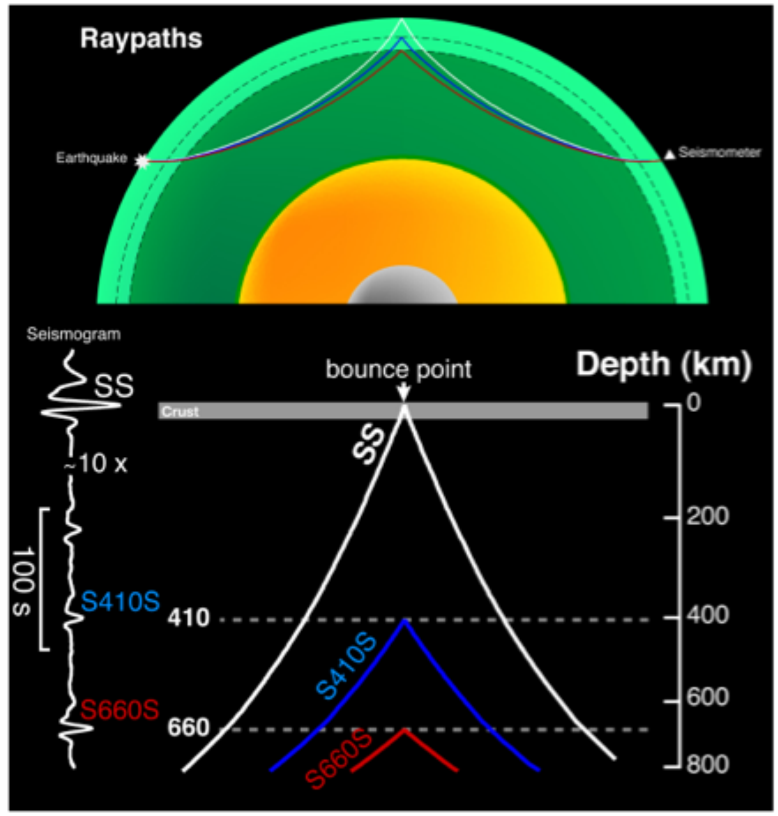

Figure by Schmerr

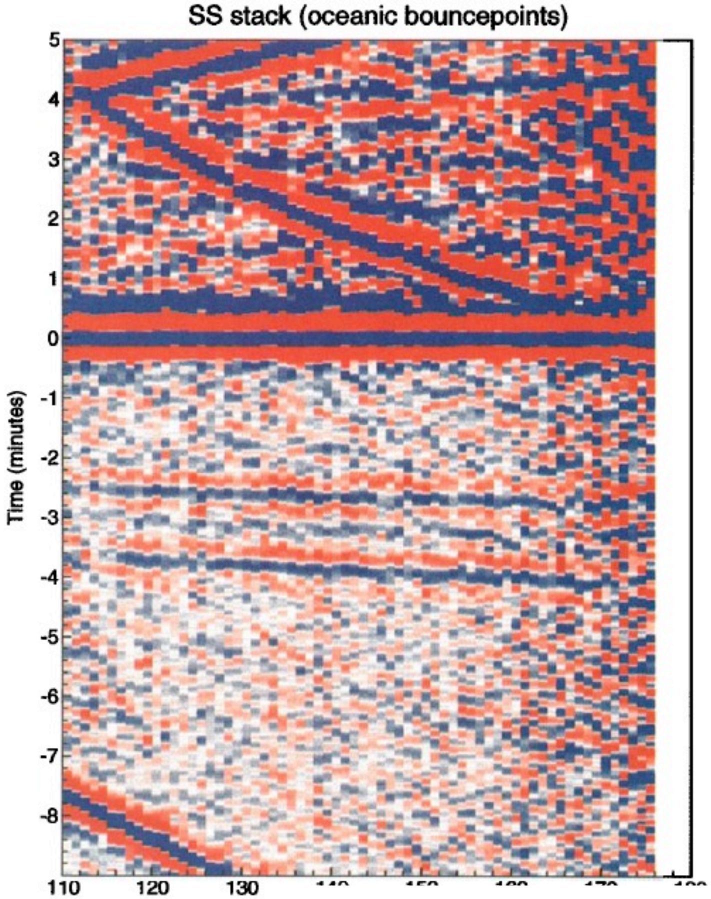

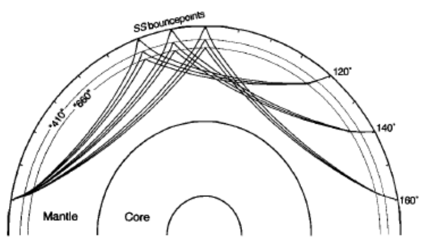

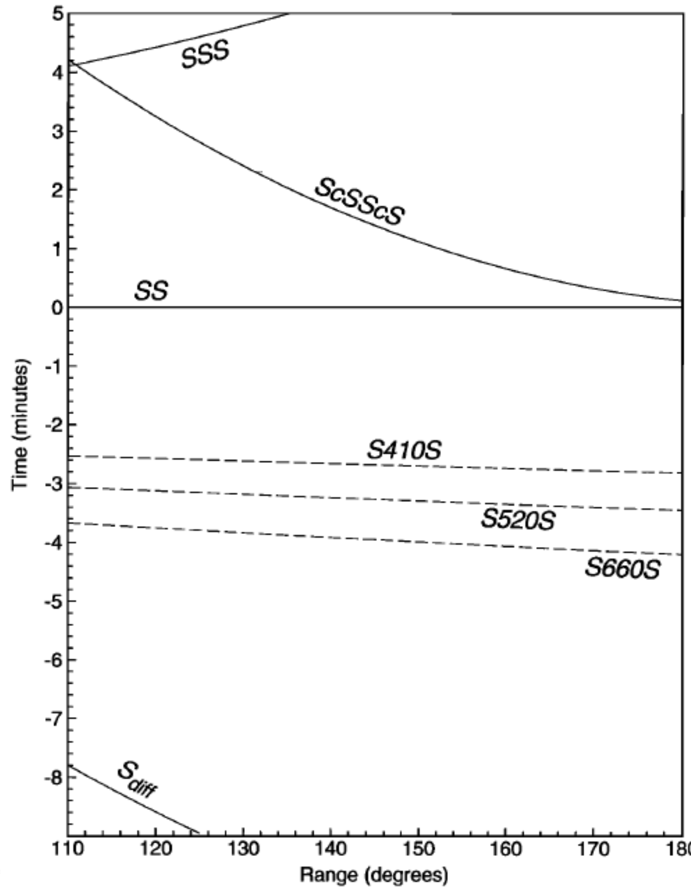

Predictions from IASP91 model

Shearer, 1996

Earth’s 1D seismic structure

- Determined from combination of body wave travel times and normal mode center frequencies
- A number of 1D Earth models have been developed: PREM (Dziewonski and Anderson, 1981), ak135 (Kennett et al., 1995), IASP91 (Kennett and Engdahl, 1991).
- Seismically fast lithosphere
- Seismically slow asthenosphere (LVZ)
- Velocity jumps at 410 and 660 km define the transition zone from the upper and lower mantle
- CMB is at ~2891 km depth
- ICB is at ~5150 km depth
- Crust on average ~30 km thick (large variations)

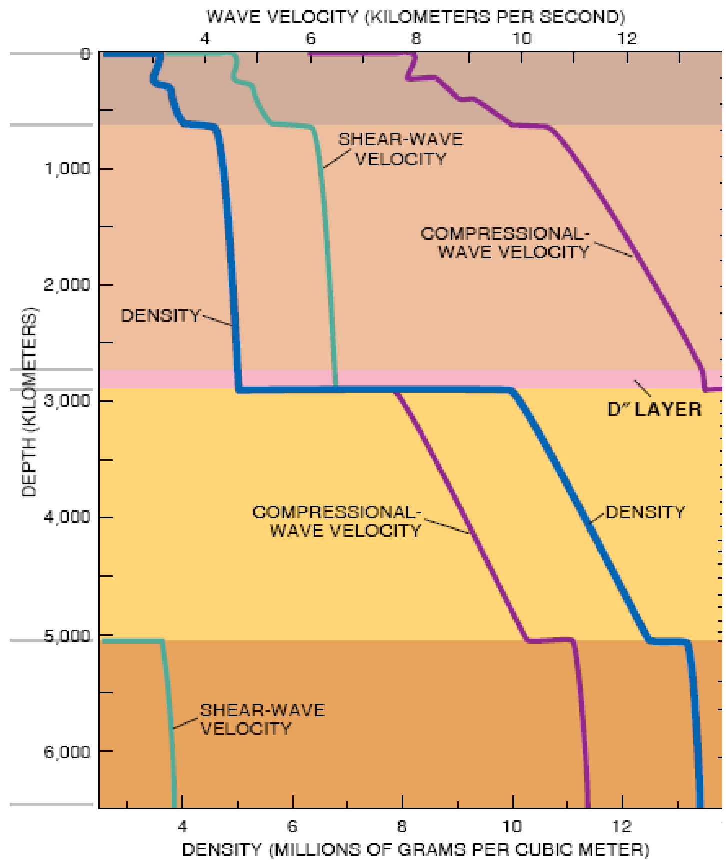

mantle

Outer core

Inner core

PREM model, Dziewonski and Anderson, 1981

“1D reference model”
First to include attenuation and radial anisotropy
+ Adams-Williamson equation

The earth's interior ~ 1980

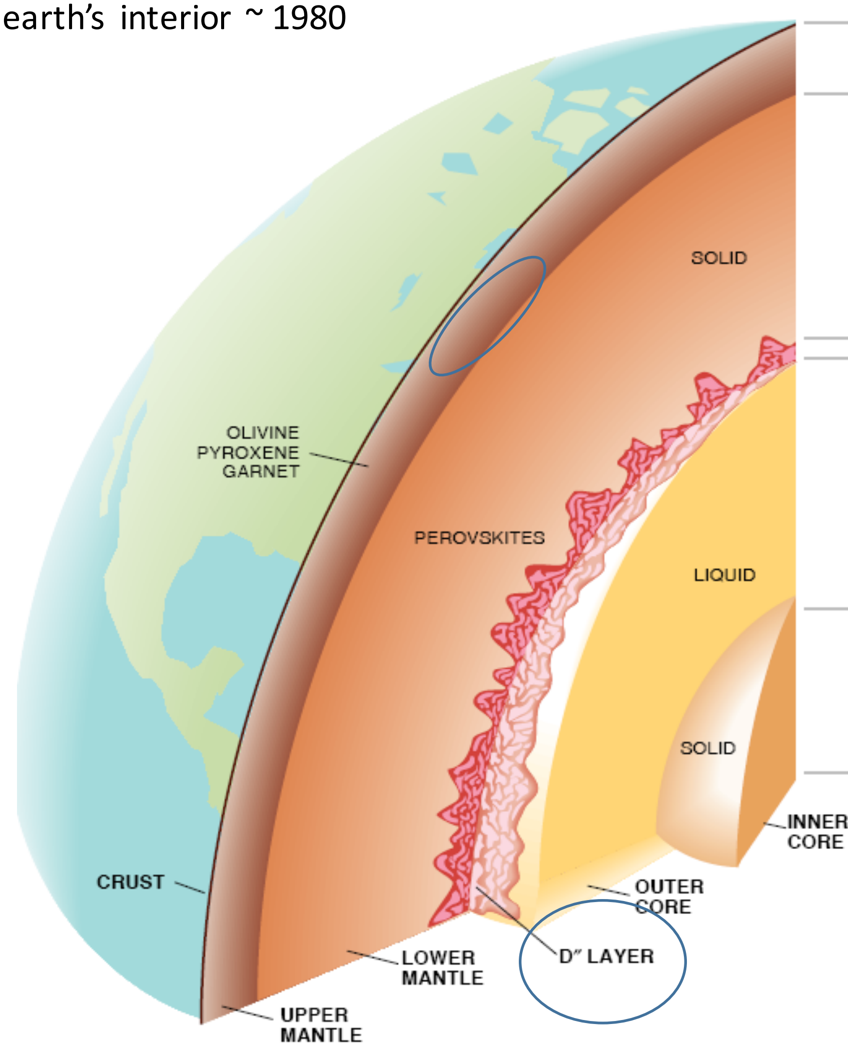

Jeanloz and Lay, Sci. Amer

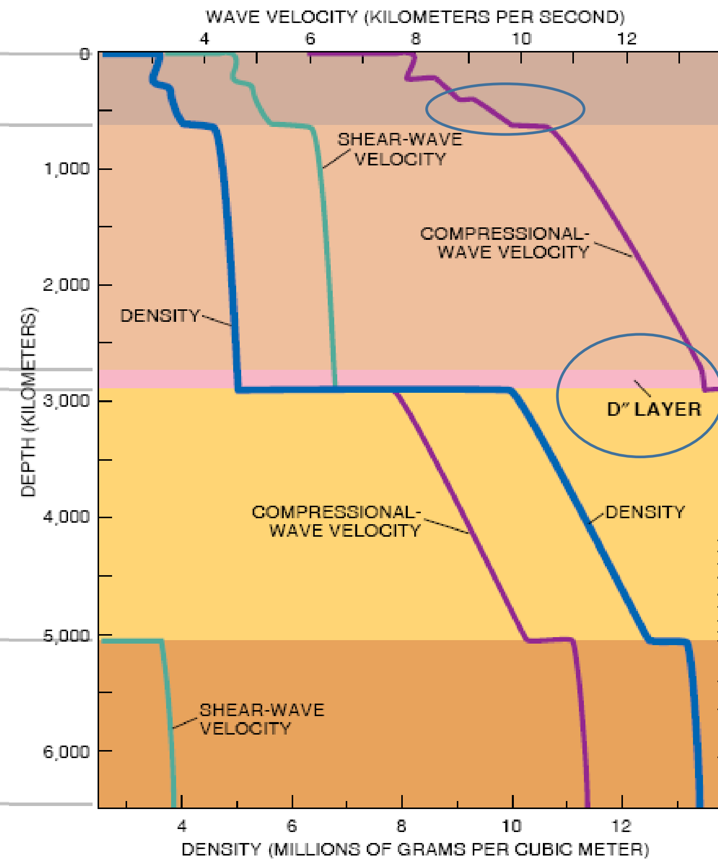

Transition zone

$(Mg,Fe)_2SiO_4$

Phase transformations

-> $(Mg,Fe)SiO_3$, $(Mg, Fe)O$

PREM model, Dziewonski and Anderson, 1981

"1D reference model"

Shallow earthquake

Figure 2.7-1: Seismograms recorded at a distance of 110°, showing surface waves.

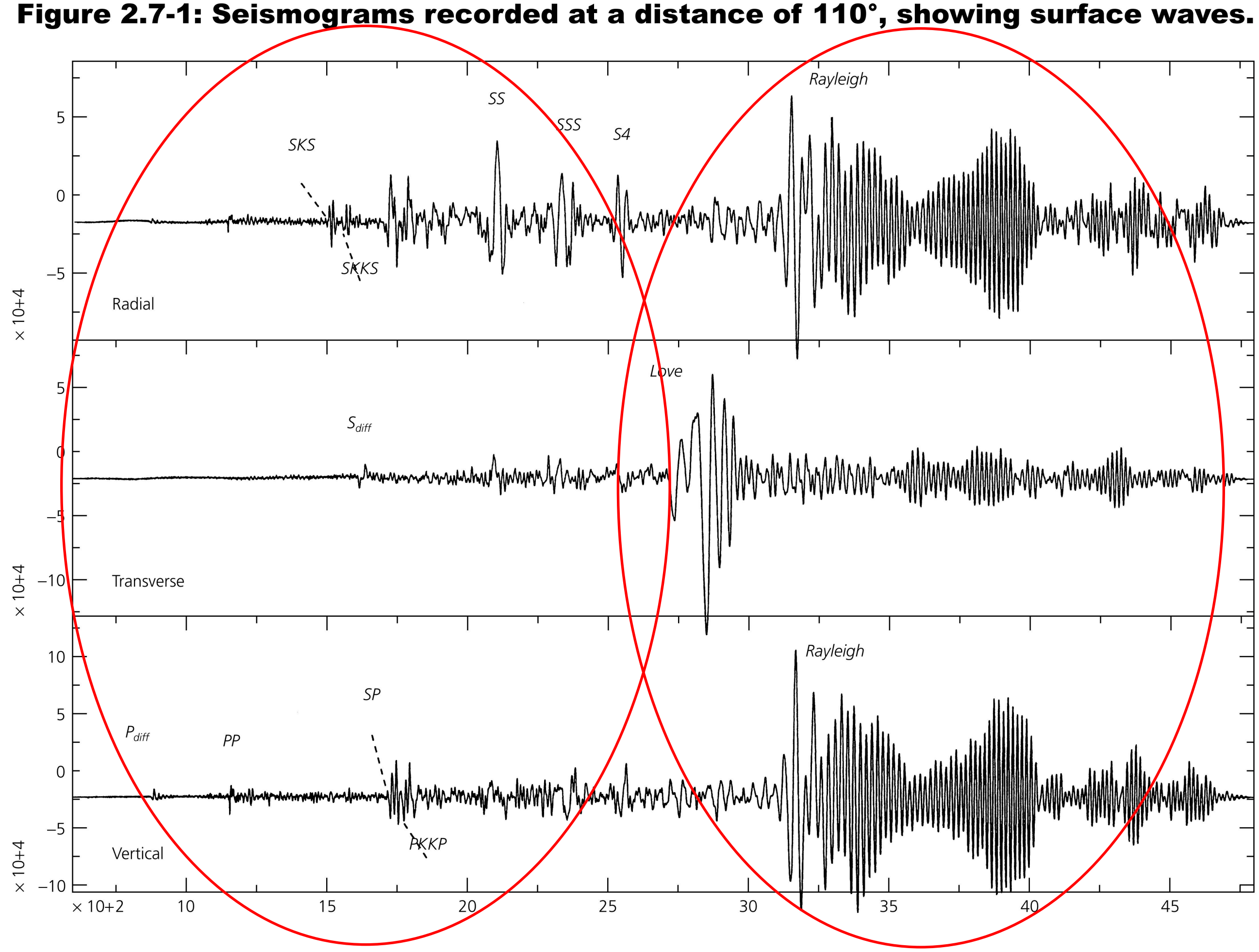

From Stein and Wysession, 2003

Surface waves

Love Waves

Particle motion is in the horizontal plane perpendicular to direction of propagation

Constructive interference between surface-bouncing SH waves

Rayleigh Waves:

Particle motion is retrograde elliptical and confined to the vertical plane joining source-receiver.

Constructive interference between post-critically reflected P and SV waves

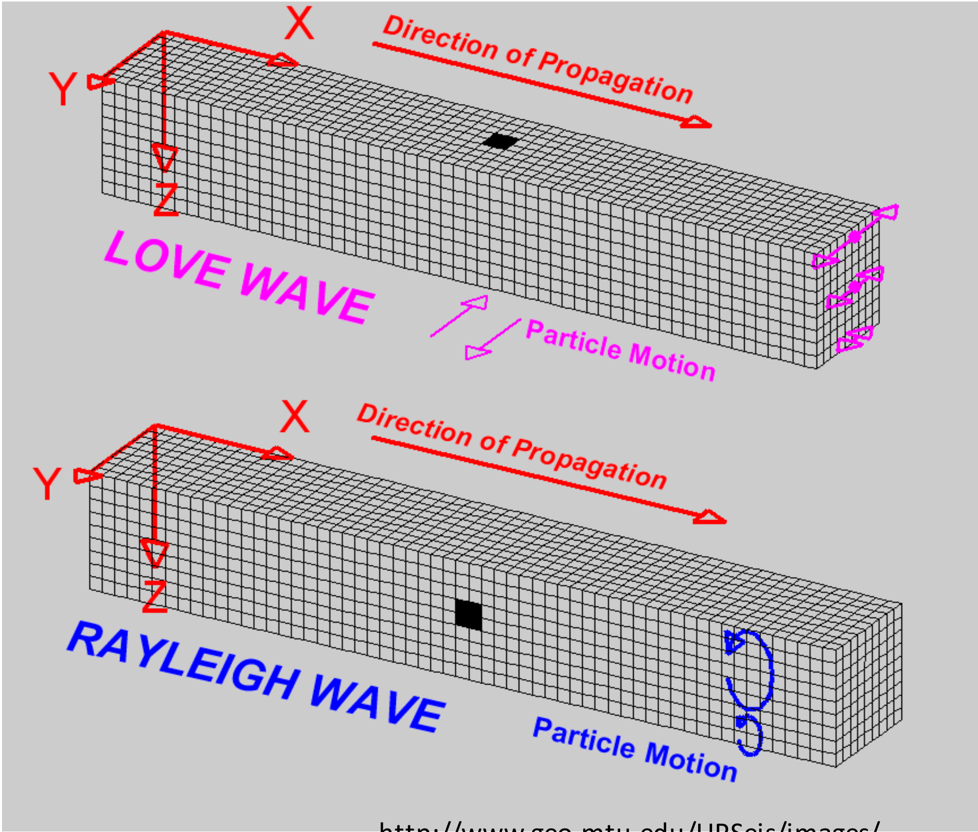

http://www.geo.mtu.edu/UPSeis/images/

Surface waves

- The amplitude of surface waves decays with depth and depends on the ratio of the depth to the wavelength.
    - => longer period (i.e. longer wavelength) surface waves tell us more about deeper parts of the mantle (T>40s)
    - => shorter period surface waves are appropriate for studying the shallow parts (crust, uppermost mantle) (10<T<40s)
- Surface waves are primarily sensitive to shear wave velocity (Vs)
- They are *dispersive* (velocity depends on period)
    - Generally longer period waves arrive first
- Most of the long period energy generated by earthquakes (T > 30s) propagates as surface waves (longer period ones are called “mantle waves”)

Surface wave dispersion

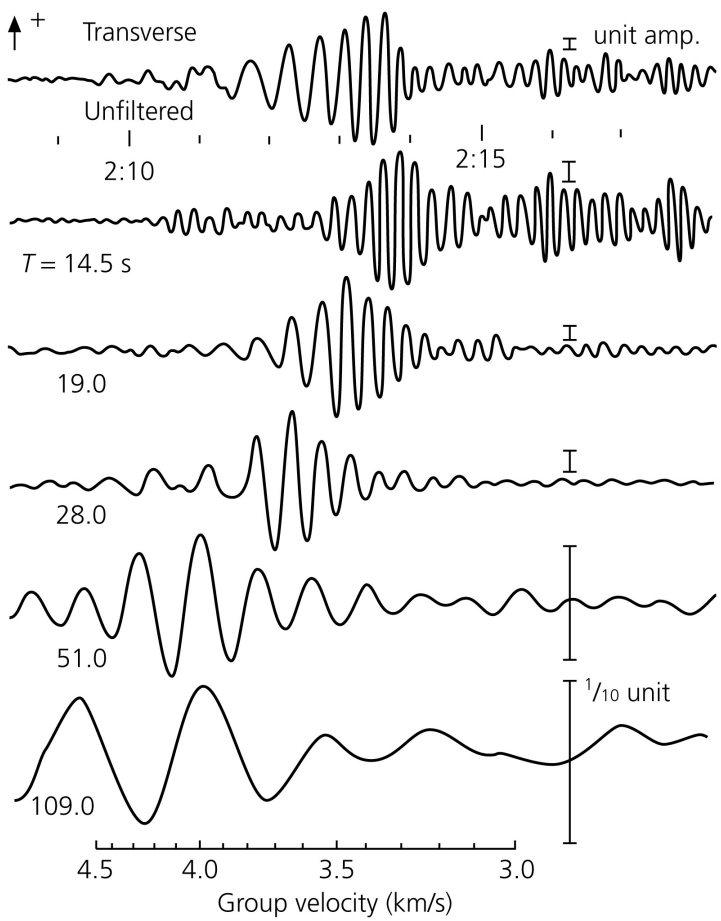

Mongolia earthquake recorded in Japan

Group velocity (U) – km/s

Velocity of travel of energy at a particular frequency

$$U = \frac{d\omega}{dk}$$

Phase velocity (C) - km/s

Velocity of travel of a particular phase (peak or trough)

$$C = \frac{\omega}{k}$$

k= 1/λ = wavenumber

Longer period surface waves travel faster
→ velocity increases with depth

Love & Rayleigh Dispersion

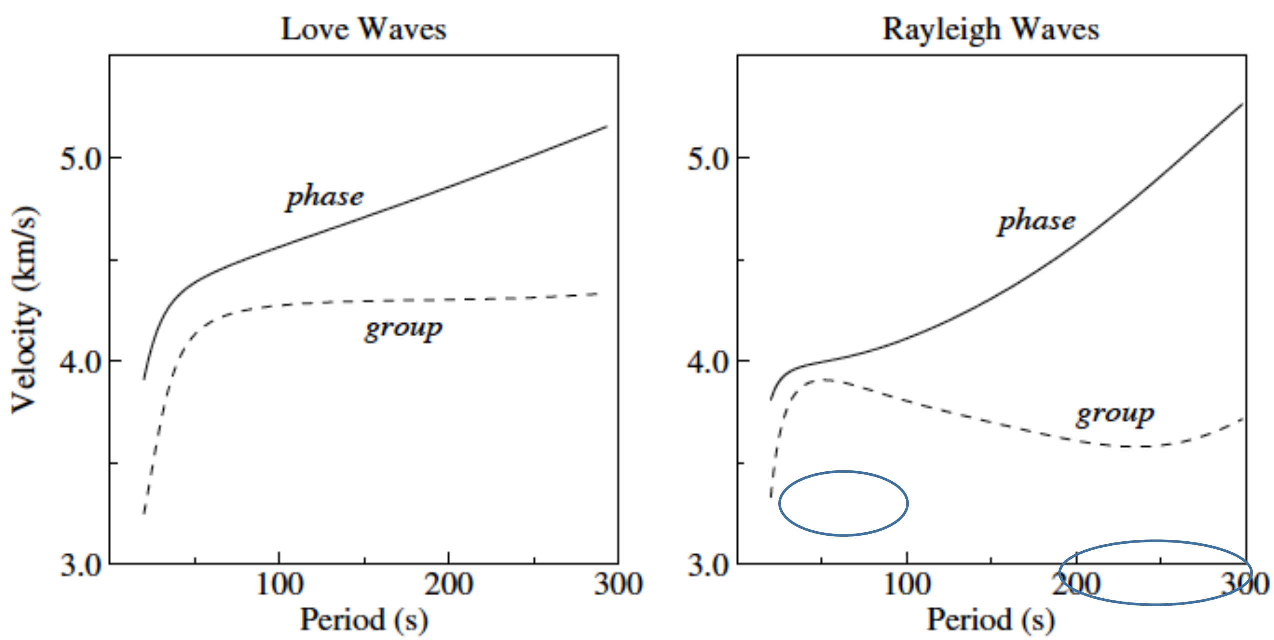

Figure 8.6 Fundamental Love and Rayleigh dispersion curves computed from the isotropic PREM model (courtesy of Gabi Laske).

At periods where group velocity attains a maximum or minimum, large amplitude surface waves are seen → "Airy" phases

figures from Shearer, 2009

Signature of plate cooling

Phase velocity measurements of Rayleigh waves allowed seismologists to infer how velocities increase with plate age (colder temperatures → faster velocities)

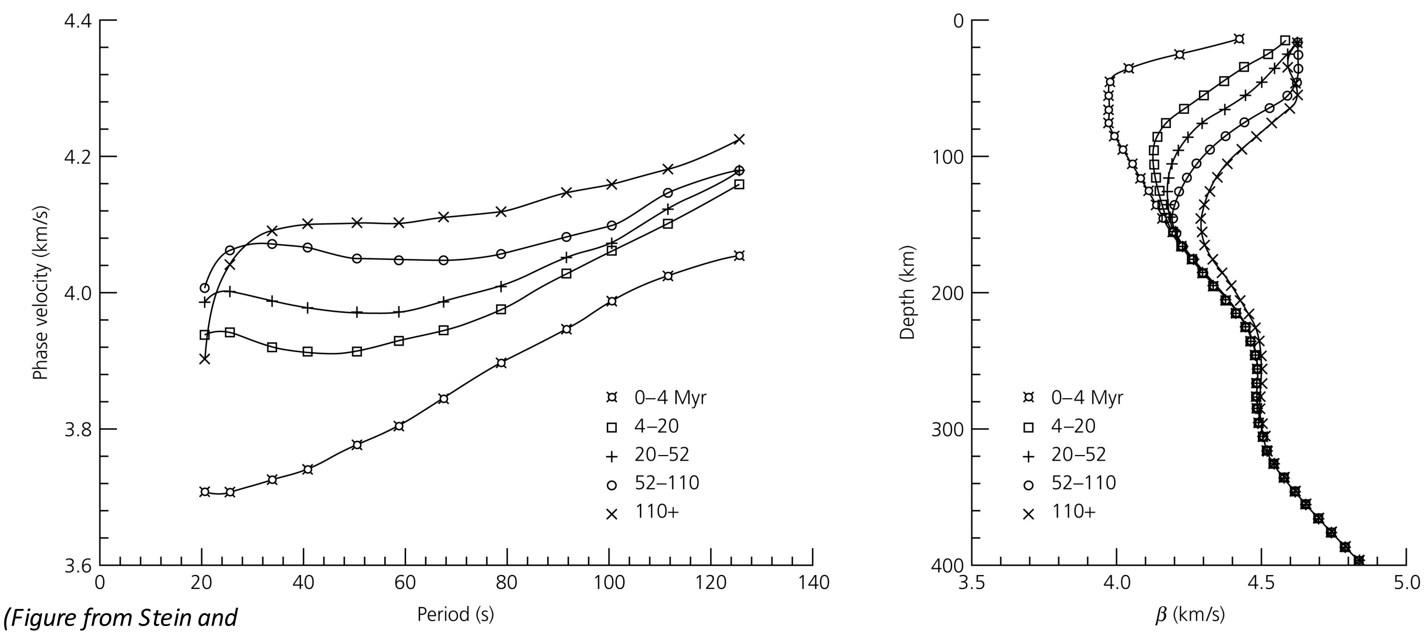

(Figure from Stein and Wysession, 2003)

Rayleigh phase velocity maps

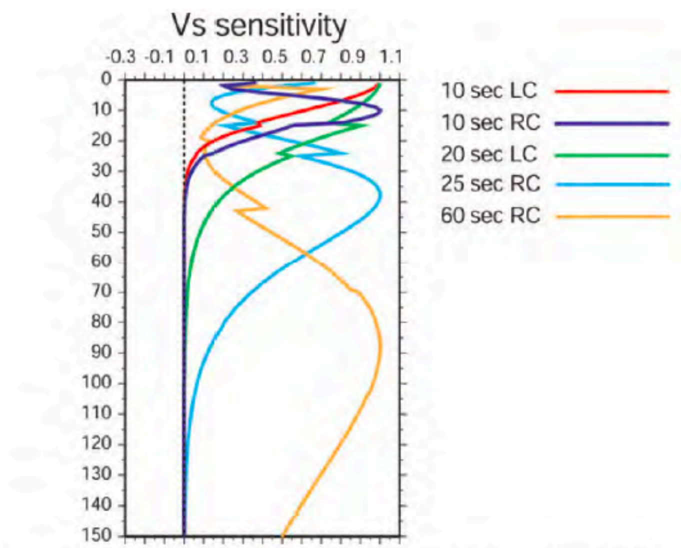

ivity kernels for Rayleigh (labelled RC) and Love (labelled LC) wave phase speeds at a selection of periods.

Period = 50 s

Period = 100 s

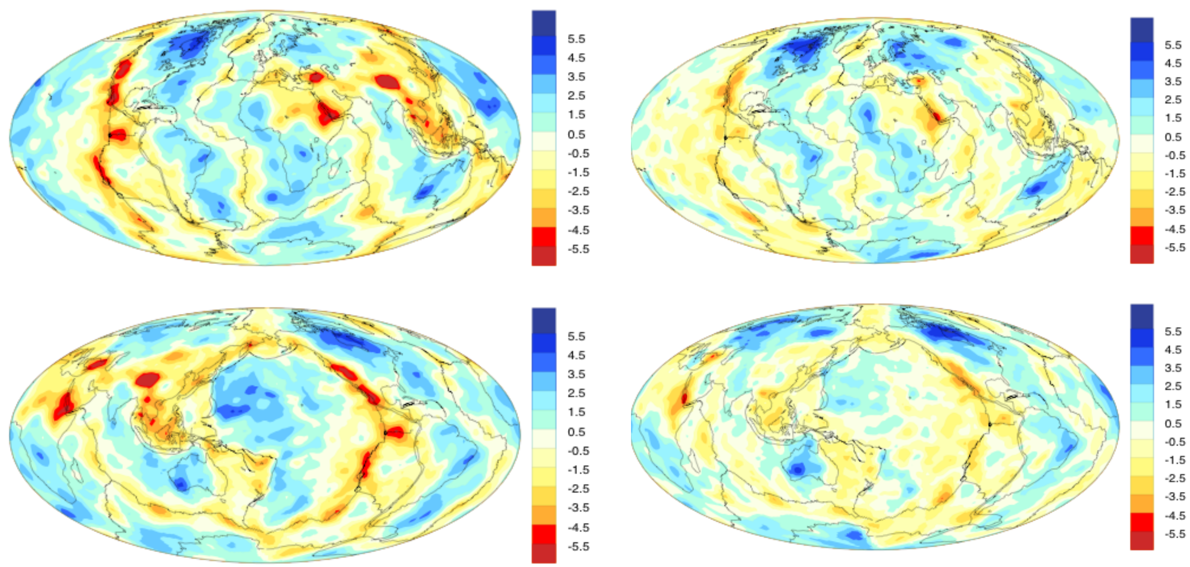

Reference: G. Masters – CIDER 2008

Exploiting ambient noise

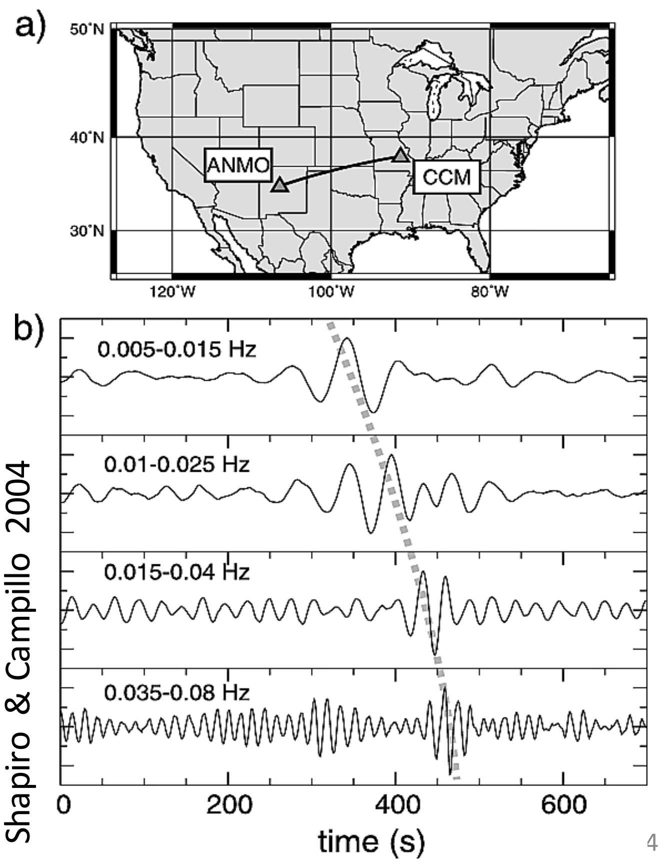

Shapiro & Campillo 2004

- Impact of ocean waves on the shores (primary microseism) and pressure variations on the ocean floor due to ocean waves (secondary microseism) create Rayleigh waves that propagate around the Earth in all directions
- By computing cross-correlations of noise at pairs of seismometers we can extract and measure Rayleigh wave dispersion
- These measurements can be used to image the Earths' interior (ambient noise tomography - ANT)

Seismic Wave attenuation

- Amplitudes of seismic waves are affected by:
  - Geometrical spreading
  - Scattering/focusing (total energy in the wavefield conserved)
  - Intrinsic attenuation (energy loss due to friction on anelastic processes).

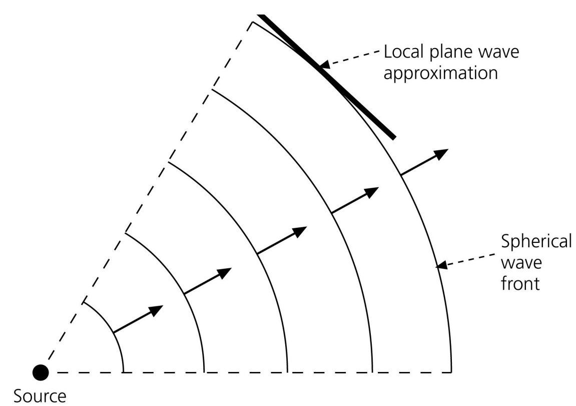

Attenuation of seismic waves

- In a perfectly elastic medium, no elastic energy would be lost during the passage of a seismic wave
- The earth is not perfectly elastic: some energy is dissipated to heat
- The quality factor Q of the medium quantifies the amount of energy lost:

$$Q^{-1} = \frac{\Delta \mathrm{E}}{2\pi \times \mathrm{E}}$$

Where E is the elastic energy of the wave
ΔE is the energy lost in a cycle

The decay of the energy of a seismic wave of period T with time (E is proportional to the amplitude-squared) can be written as:

$$E = E_0 e^{-2\pi t/TQ}$$

In terms of amplitude:

$$A = A_0 e^{-\pi t/TQ}$$

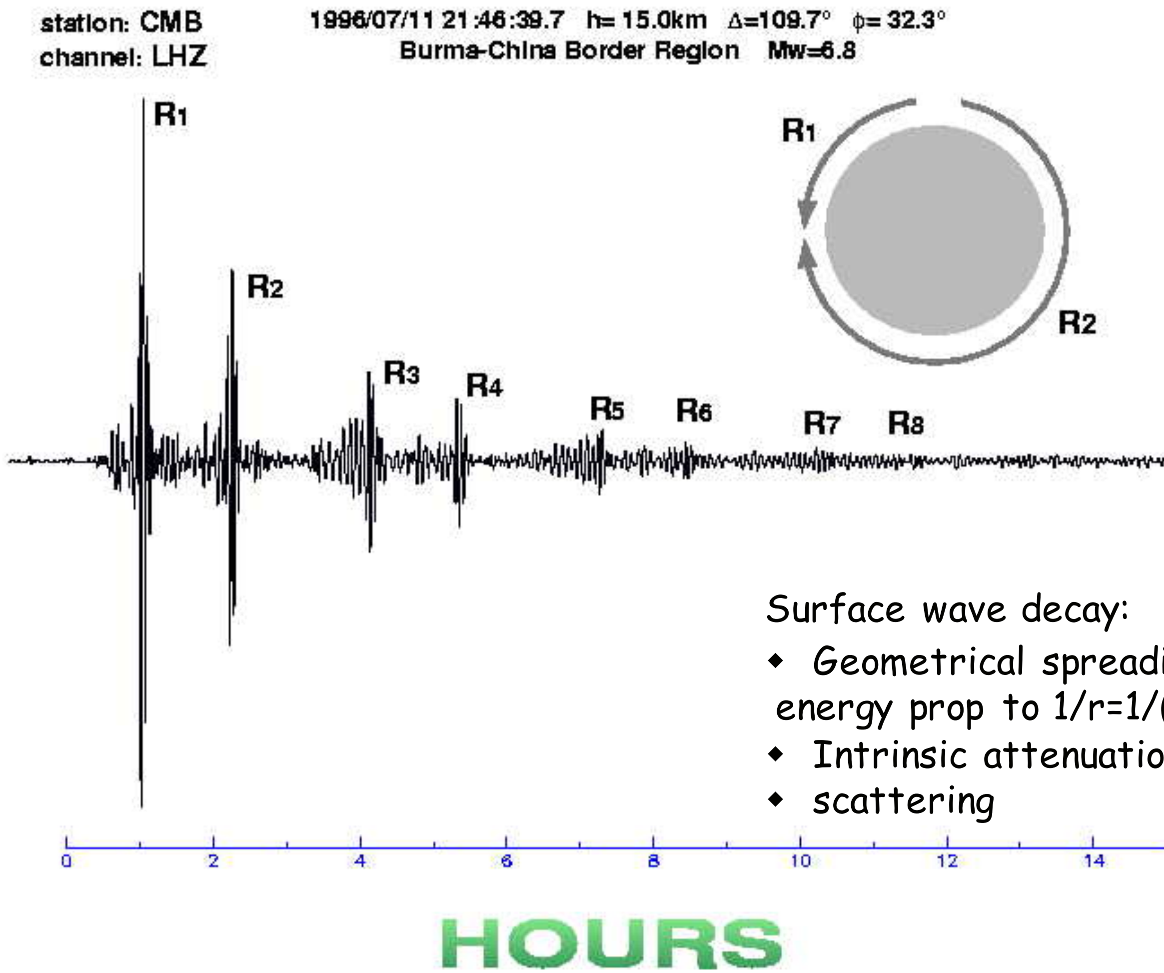

Surface wave decay:

- Geometrical spreading energy prop to $1/r=1/(a\sin\Delta)$
- Intrinsic attenuation
- scattering

Figure 3.7-10: Comparison of seismograms on the earth and moon.

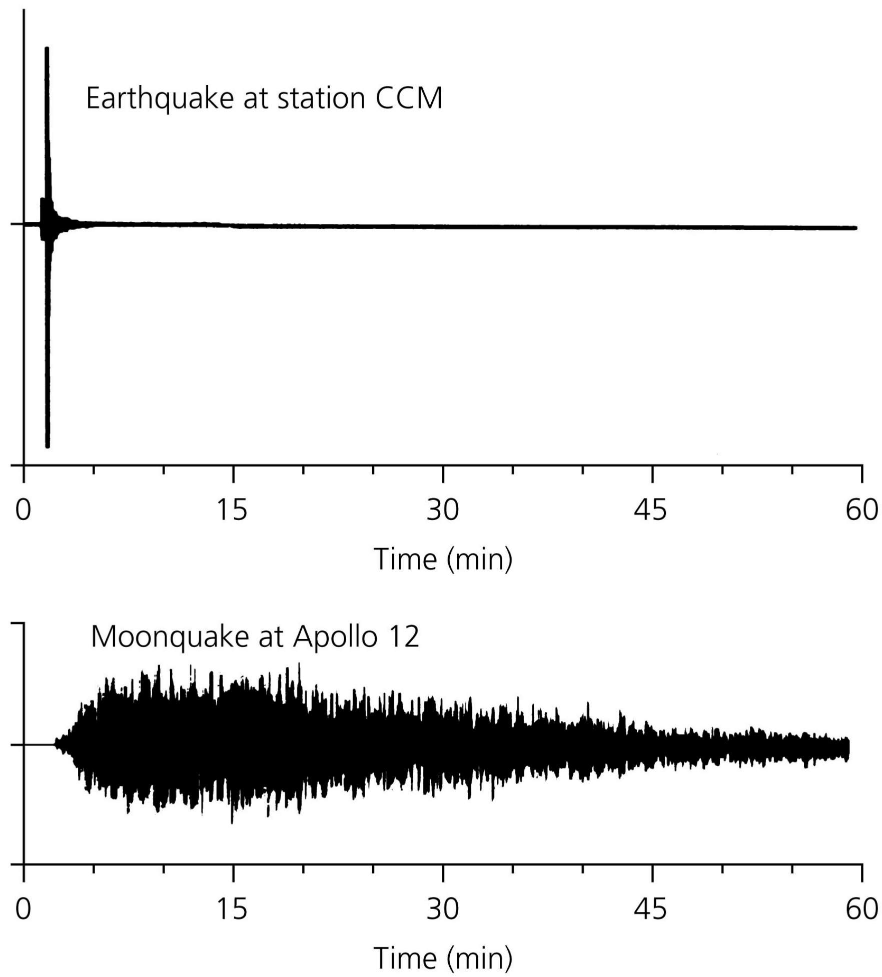

Stein and Wysession, 2003

Earth attenuation structure

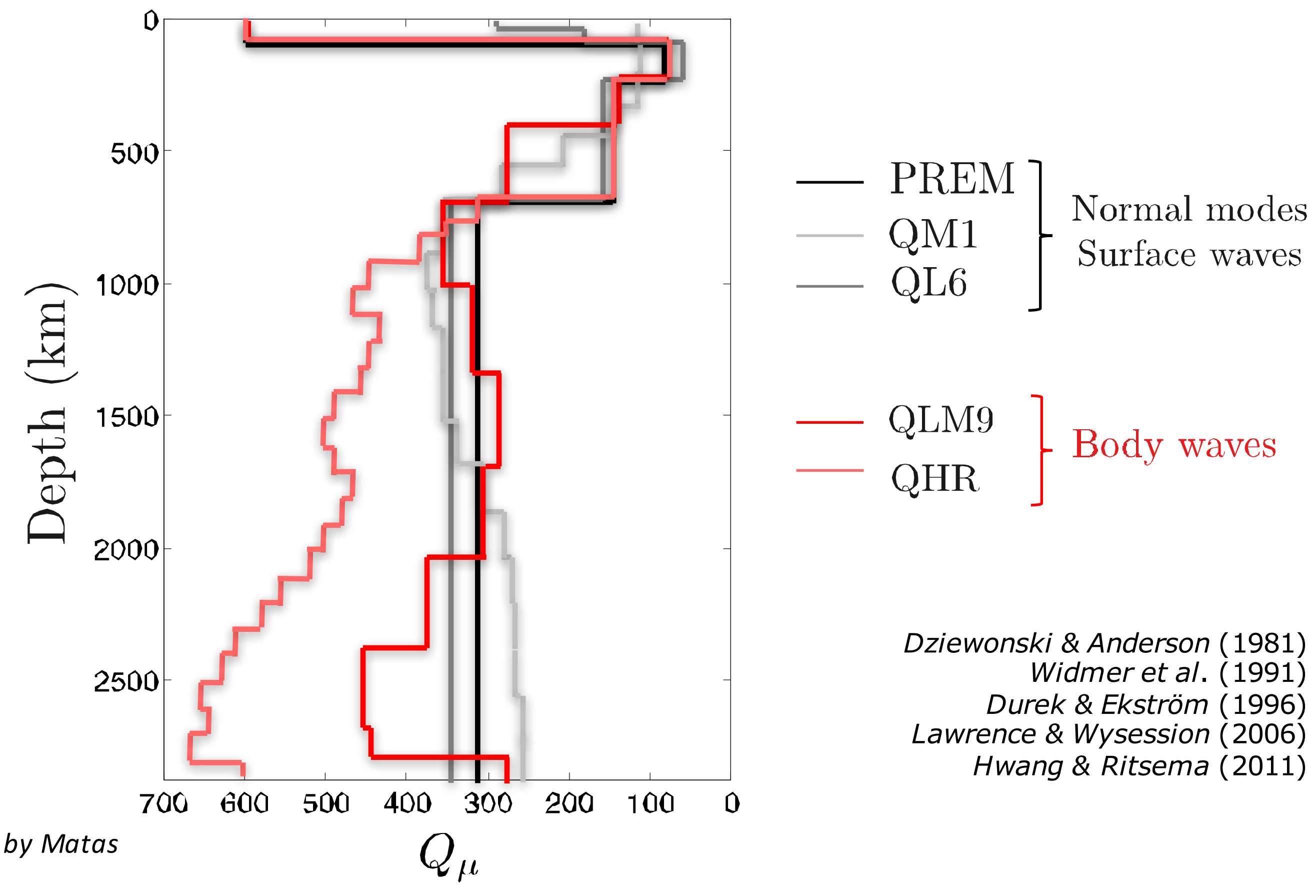

Dziewonski & Anderson (1981)
Widmer et al. (1991)
Durek & Ekström (1996)
Lawrence & Wysession (2006)
Hwang & Ritsema (2011)

figure by Matas

Dispersion due to attenuation

Absorption band model for the Earth

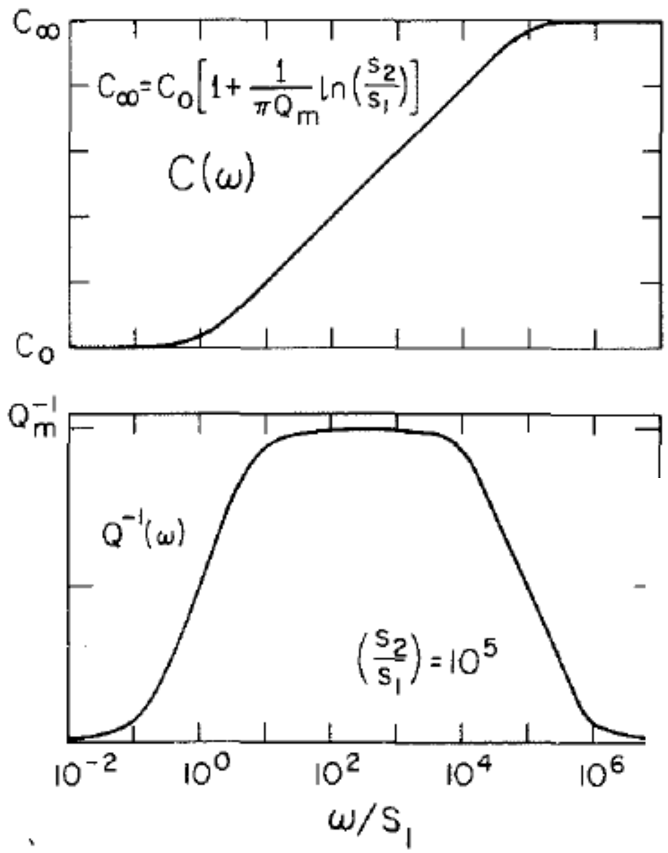

Kanamori and Anderson, 1977

Velocity dispersion due to attenuation:

$$C(\omega) = C_0\left[1 + \frac{1}{\pi Q_m}\ln\left(\frac{\omega}{s_1}\right)\right]$$

$$C(\omega) = C_\infty\left[1 - \frac{1}{\pi Q_m}\ln\left(\frac{s_2}{\omega}\right)\right]$$

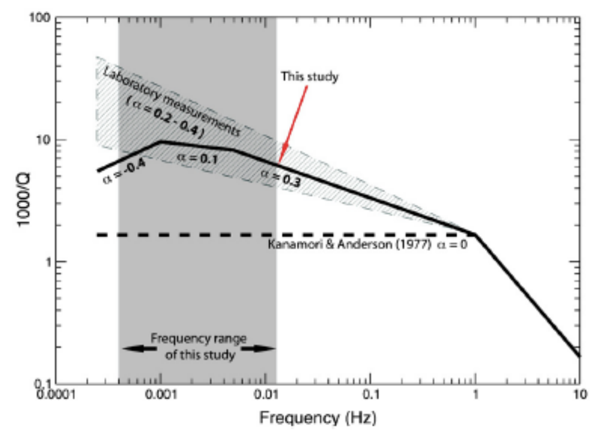

Lekic, Matas, Panning and Romanowicz, EPSL, 2009

Examples of focusing

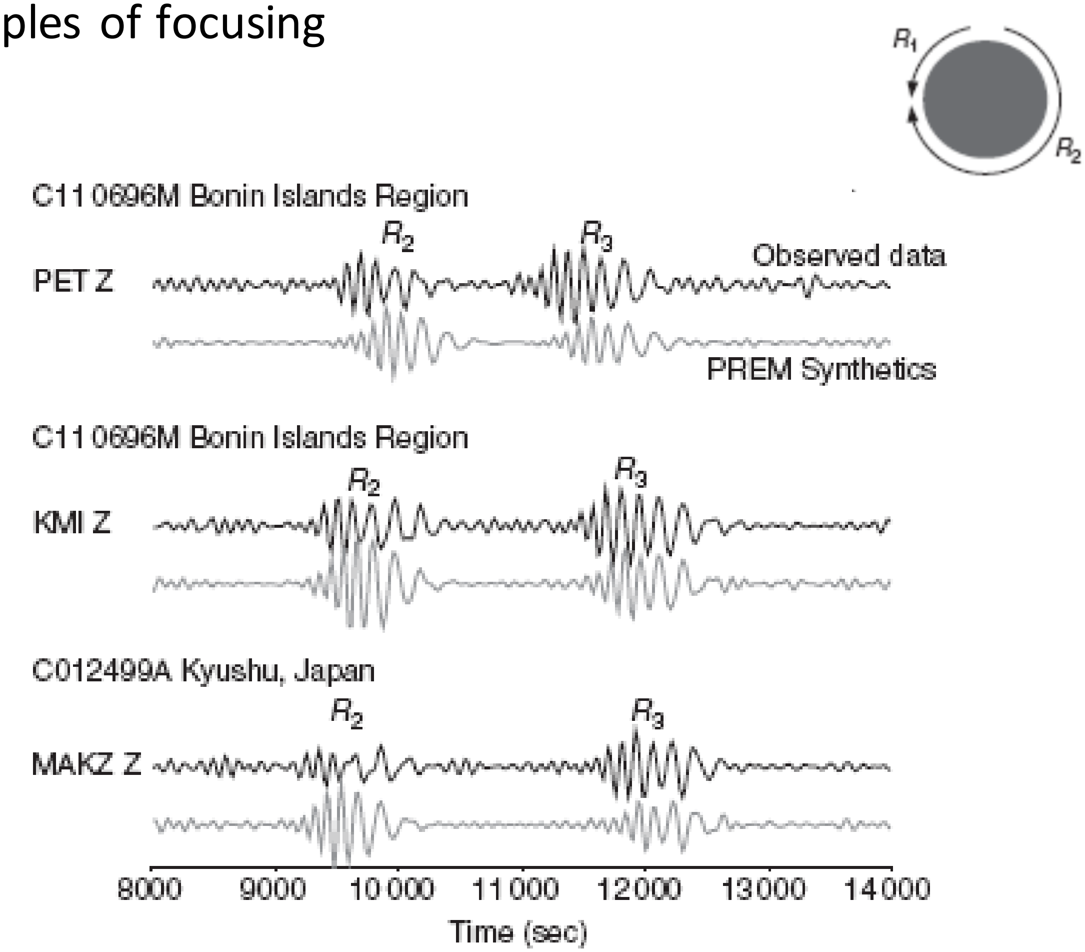

The earth's interior
~ 1980

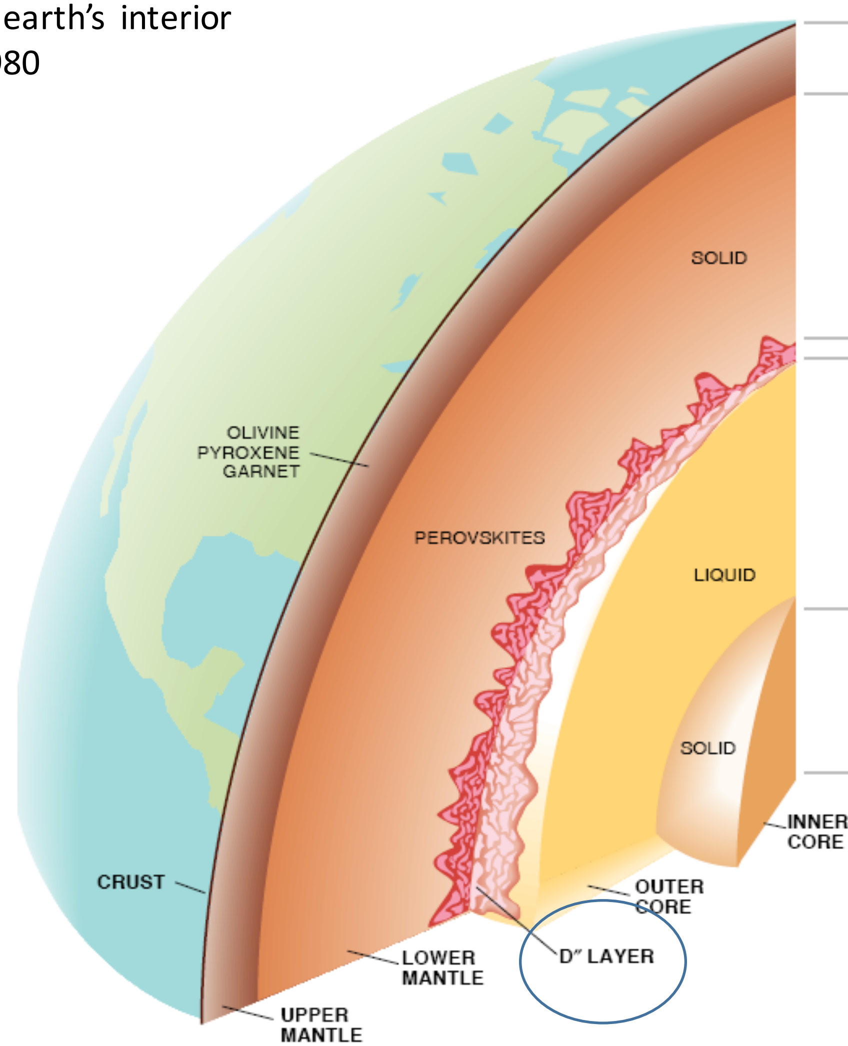

Jeanloz and Lay, Sci. Amer

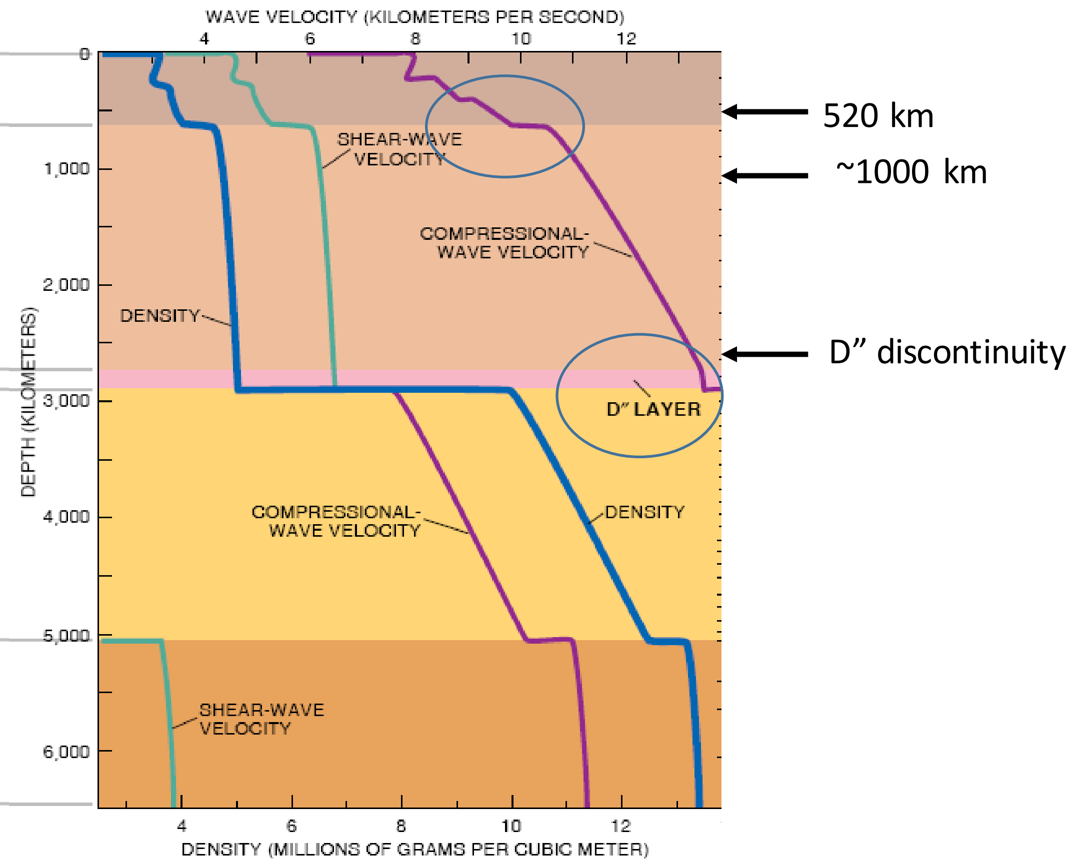

PREM model, Dziewonski and Anderson, 1981

Detection of a seismic discontinuity at ~520 km depth -→ Wadsleyite to Ringwoodite

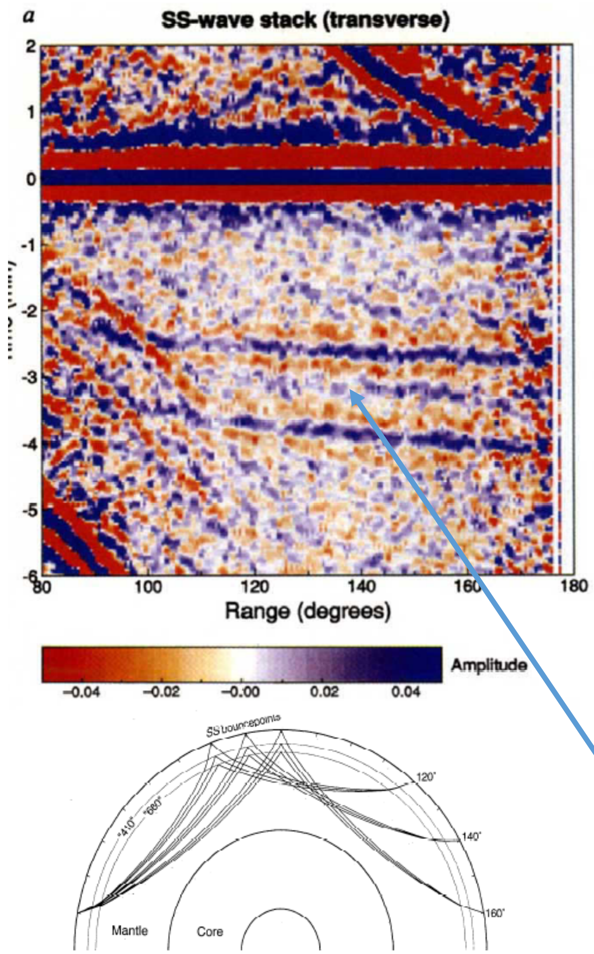

Shearer, 1990 Nature; 1991

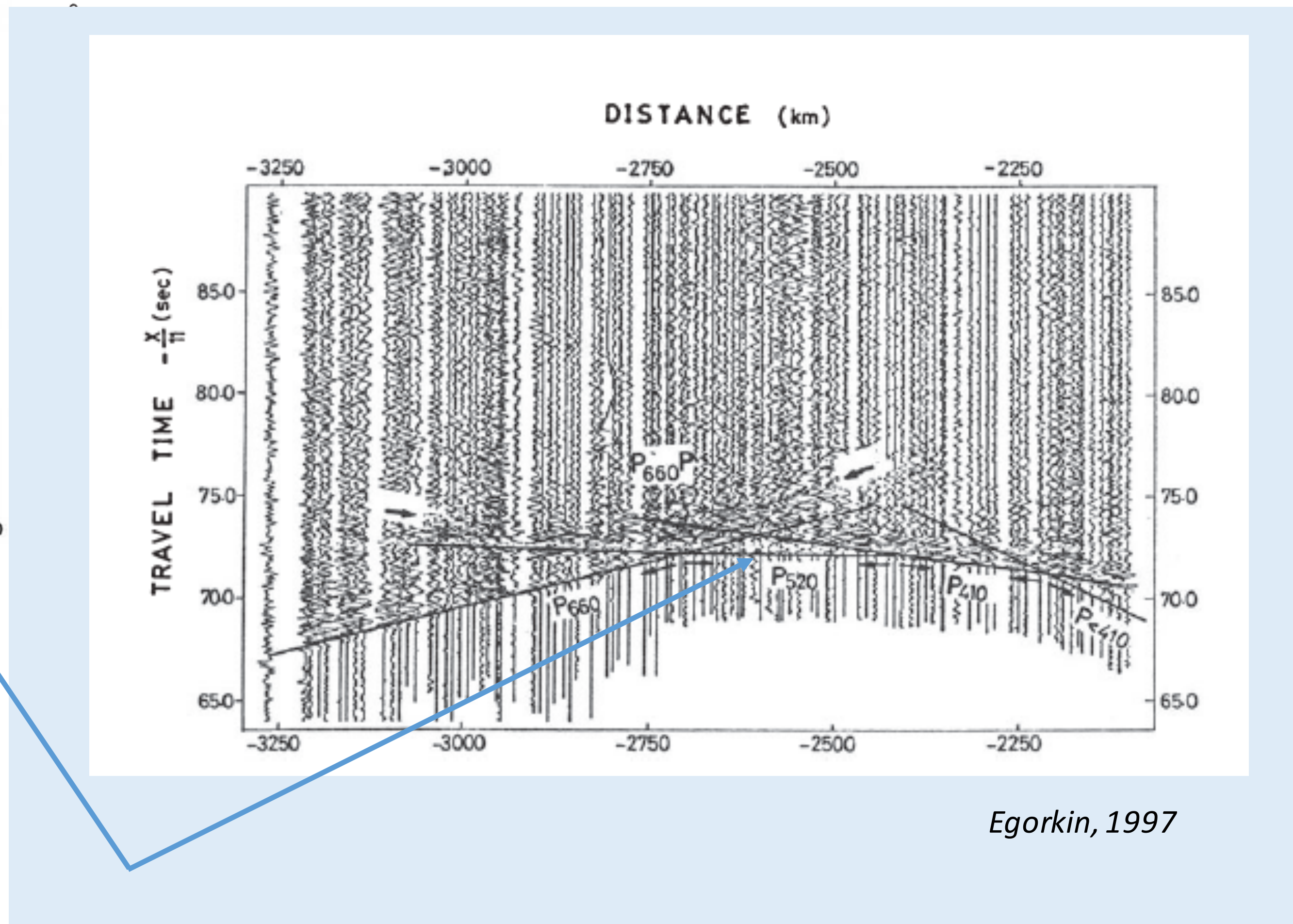

Egorkin, 1997

Detection of a seismic discontinuity at ~520 km depth -→ Wadsleyite to Ringwoodite

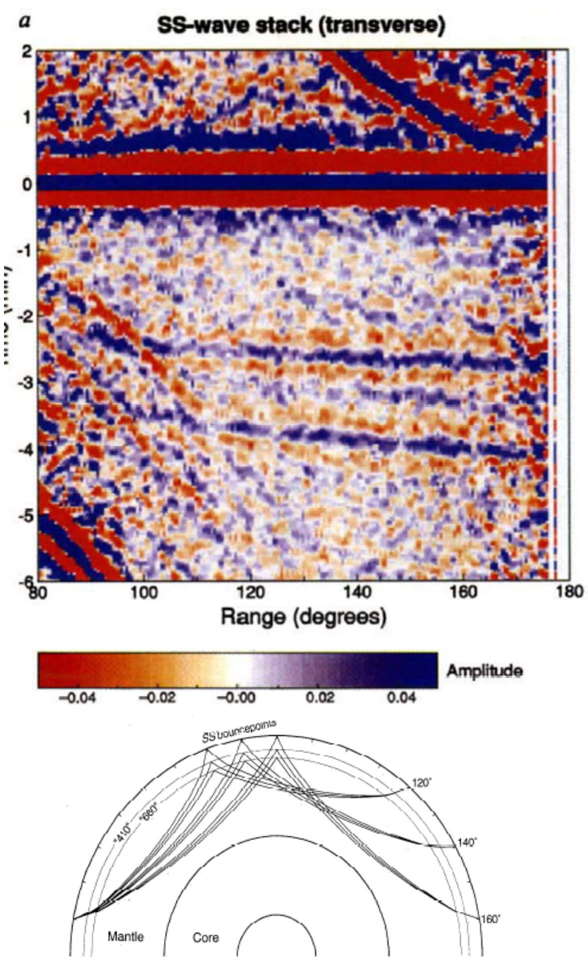

Shearer, 1990 Nature;

Topography of 520 consistent with the Wadsleyite to Ringwoodite transition + compositional heterogeneity

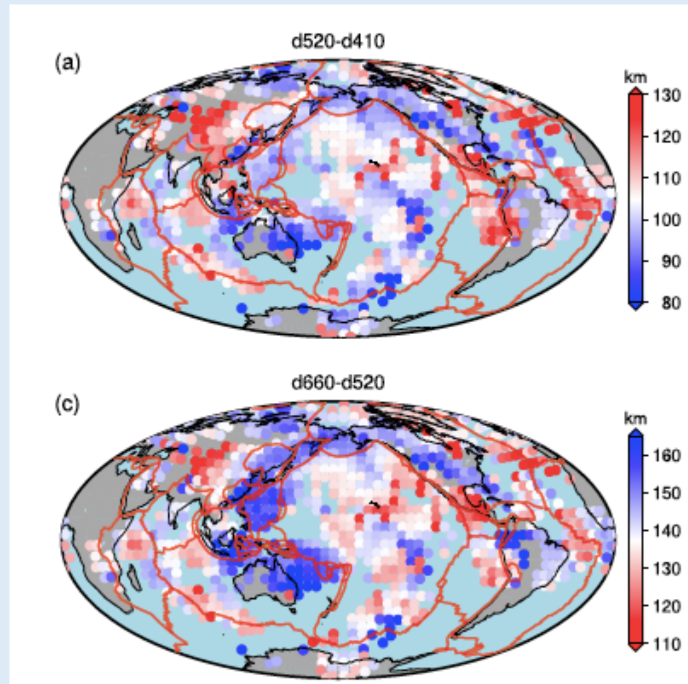

Tian et al., EPSL 2020

1983

A lower mantle *S*-wave triplication and the shear velocity structure of D″

Thorne Lay and Donald V. Helmberger *Seismological Laboratory, California Institute of Technology, Pasadena, California 91125, USA*

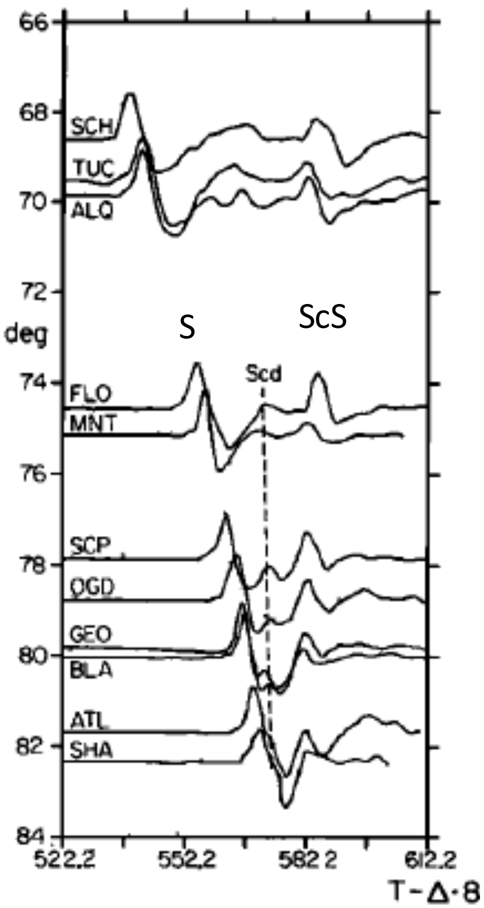

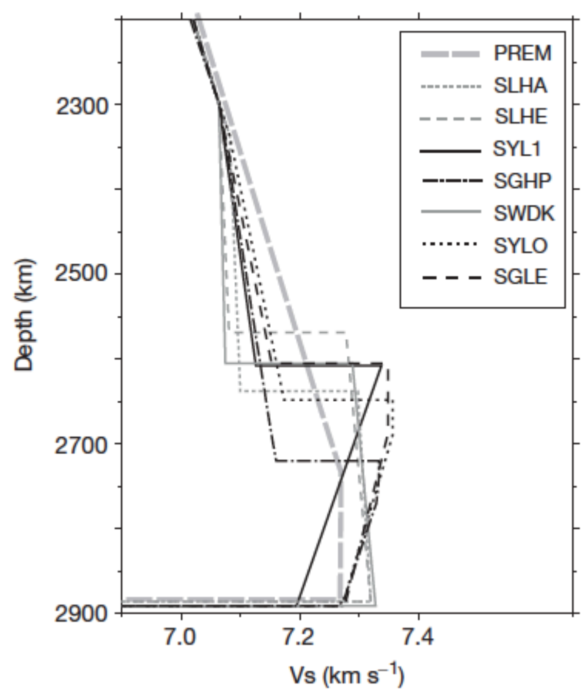

D″ Discontinuity

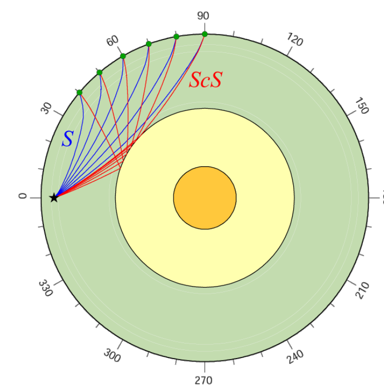

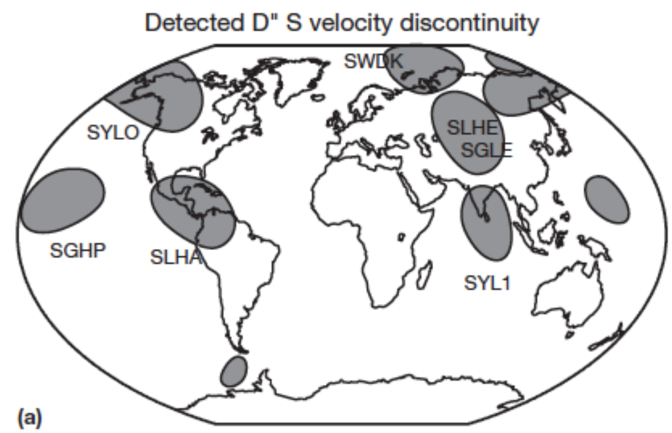

Lay, ToG, 2015

2004

Post-Perovskite Phase Transition in $MgSiO_3$

Motohiko Murakami,[1*] Kei Hirose,[1*] Katsuyuki Kawamura,[1] Nagayoshi Sata,[2] Yasuo Ohishi[3]

SCIENCE VOL 304 7 MAY 2004

Theoretical and experimental evidence for a post-perovskite phase of $MgSiO_3$ in Earth's D″ layer

Artem R. Oganov[1] & Shigeaki Ono[2]

NATURE | VOL 430 | 22 JULY 2004

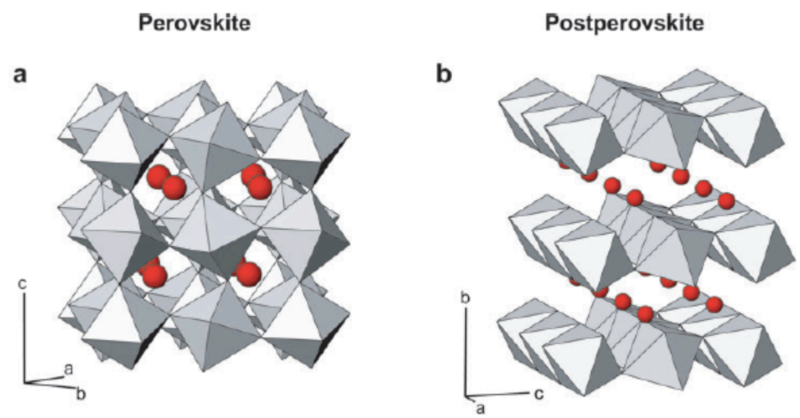

Shim, Annu. Rev., 2009

Some uncertainties remain on the Clapeyron slope and the depth of the transition in the real earth

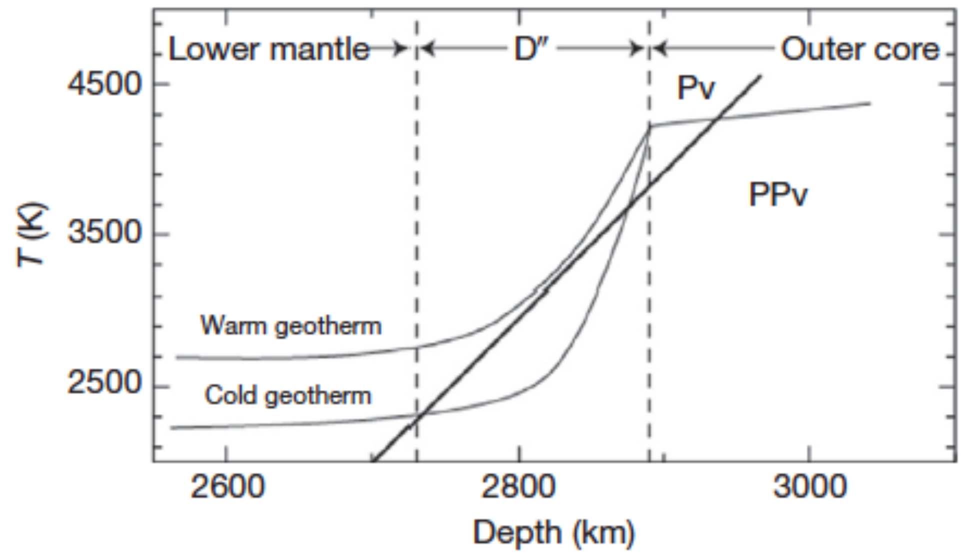

Hernlund et al., Nature, 2005

pPv may only exist in cold regions of D"

1986 The solid inner core is anisotropic

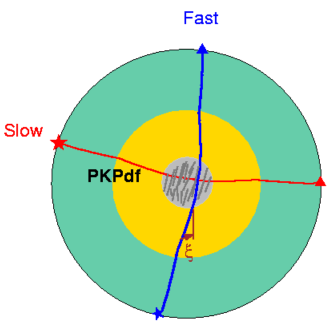

GEOPHYSICAL RESEARCH LETTERS, VOL. 13, NO. 13, PAGES 1545-1548, DECEMBER 1986

ANISOTROPY OF THE INNER CORE INFERRED FROM *PKIKP* TRAVEL TIM

Andrea Morelli, Adam M. Dziewonski and John H. Woodhouse

Department of Earth and Planetary Sciences, Harvard University

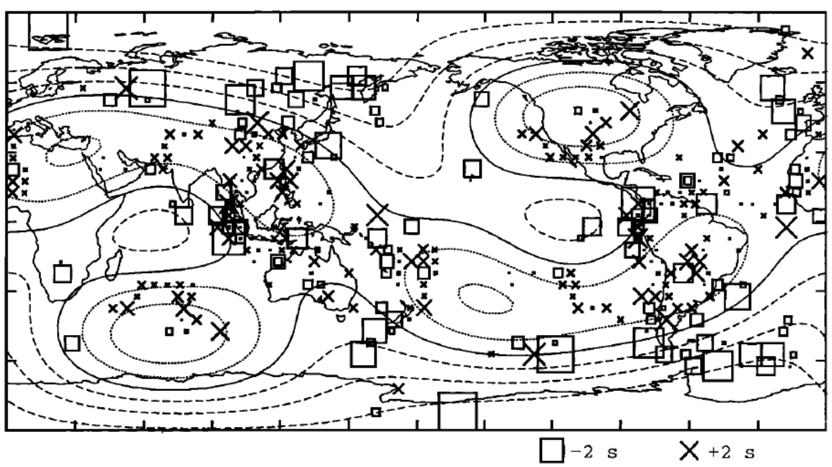

Fig. 1. Travel-time anomalies for nearly vertical rays (170° – 180°) after correction for station anomalies and lower mantle and CMB structures. Each symbol is the average in a bin of a subdivision of 1654 equi-areal cells. Each residual is plotted both at the source and receiver locations. The spherical harmonic expansion truncated at degree 4 is shown by the contour lines; contour interval is 0.4 s.

GEOPHYSICAL RESEARCH LETTERS, VOL. 13, NO. 13, PAGES 1549-1552, DECEMBER 1986

EVIDENCE FOR INNER CORE ANISOTROPY FROM FREE OSCILLATIONS

John H. Woodhouse, Domenico Giardini and Xiang-Dong Li

Department of Earth and Planetary Sciences, Harvard University

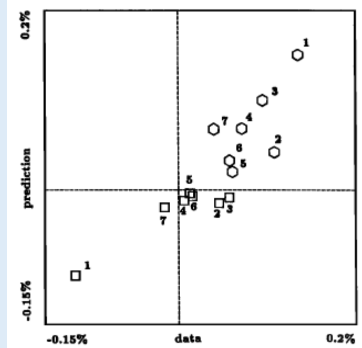

Fig. 4. Data and theoretical predictions are compared for the homogeneous, axially symmetric model of anisotropy having radial dependence proportional to r^2 – see text. Degree 2 coefficients are indicated by hexagons and degree 4 coefficients by squares.

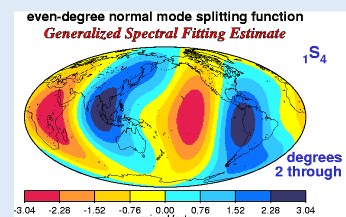

Mantle mode

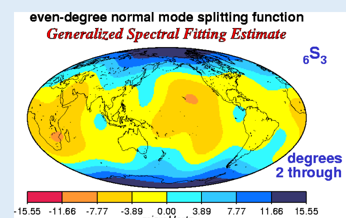

Core mode

Hemispherical dependence of anisotropy in the inner core

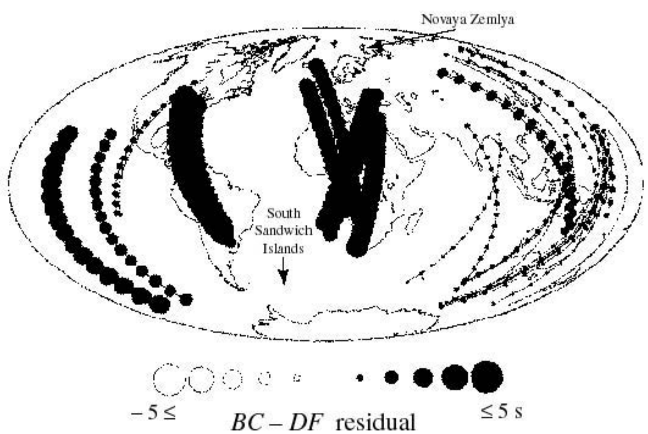

Tanaka and Hamaguchi, 1995

From PKP phases

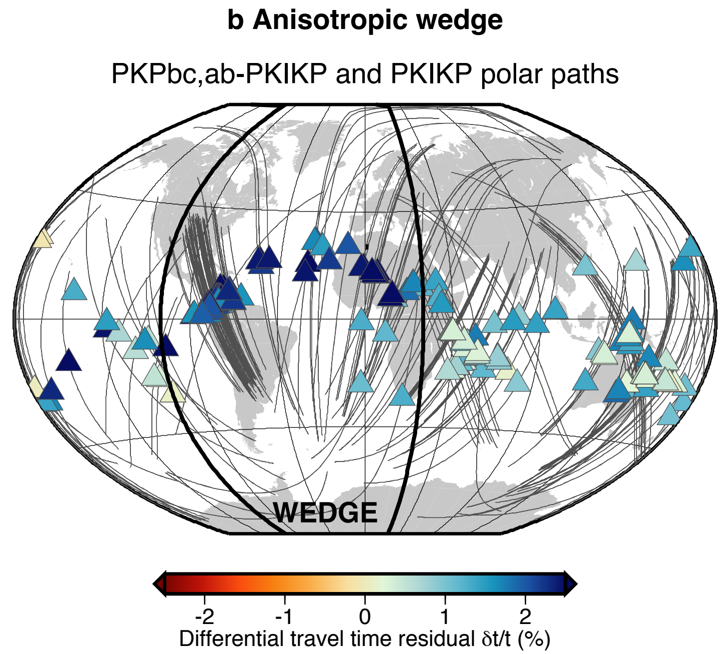

Deuss, *Annu. Rev*, 2014

From coupled normal modes:

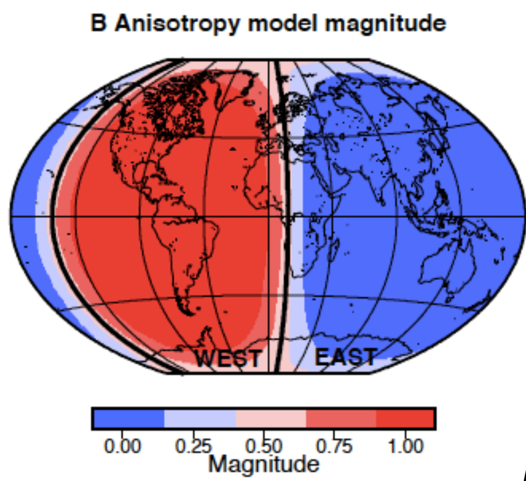

Deuss et al., 2010

Inner core super rotation?

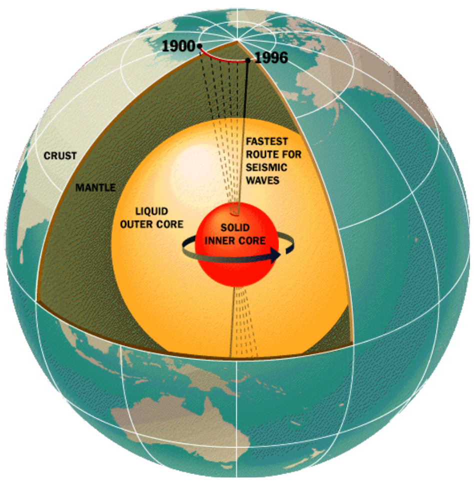

Song & Richards (1996):
Inner core spins faster than rest of the planet, with speed of up to 1° per year

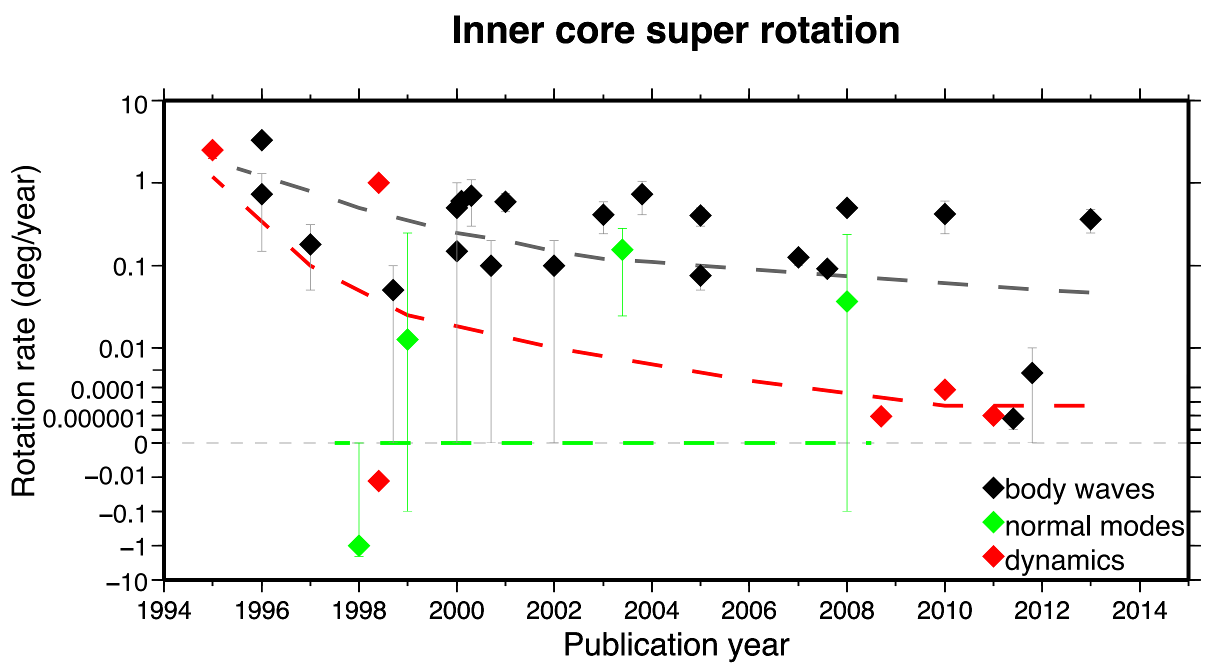

(Deuss, *Annu. Rev.*, 2014)

Now "settled" <0.01°/yr

1977 onwards

Seismic tomography

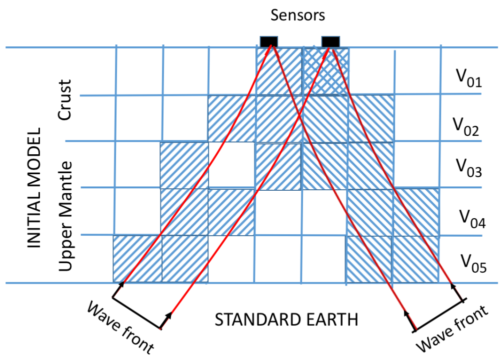

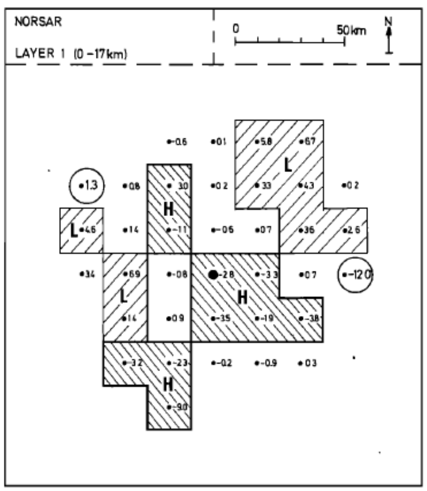

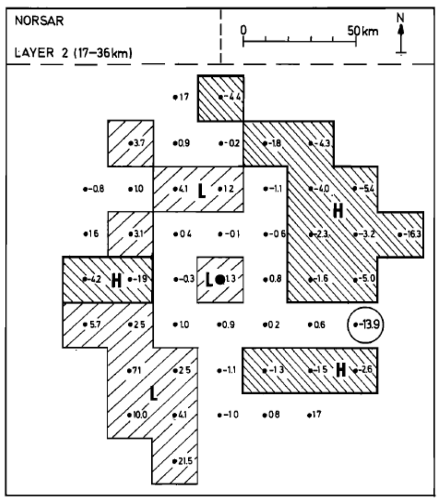

Aki, Christofferson and Husebye, 1977: “ACH”

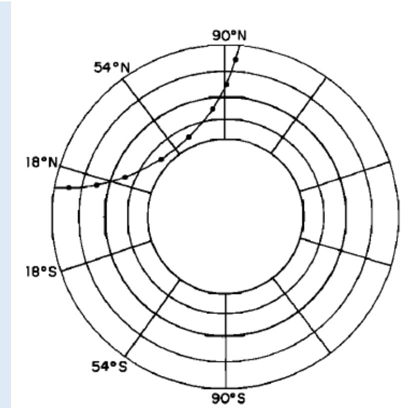

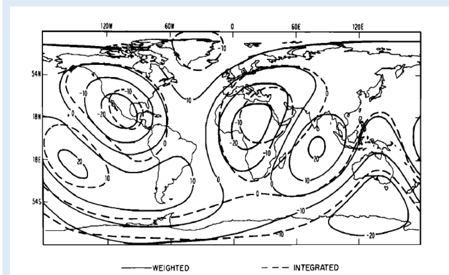

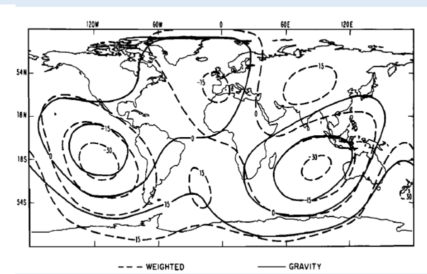

670-1100 km

2200 - CMB

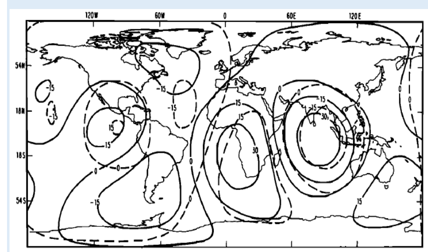

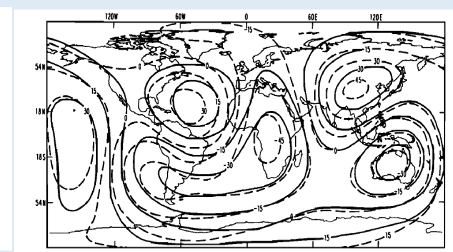

Dziewonski, Hager and O’Connell (1977)

1977-1984

Model L02.56 (Vp)

Dziewonski, 1984

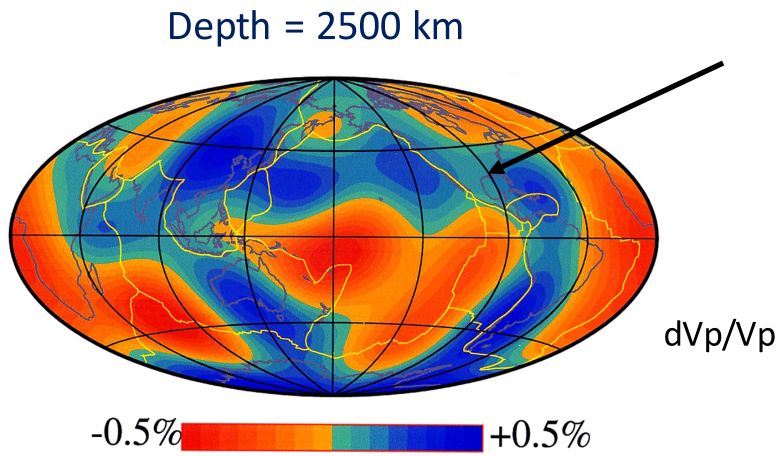

Model M84C (Vs)

Woodhouse and Dziewonski, 1984

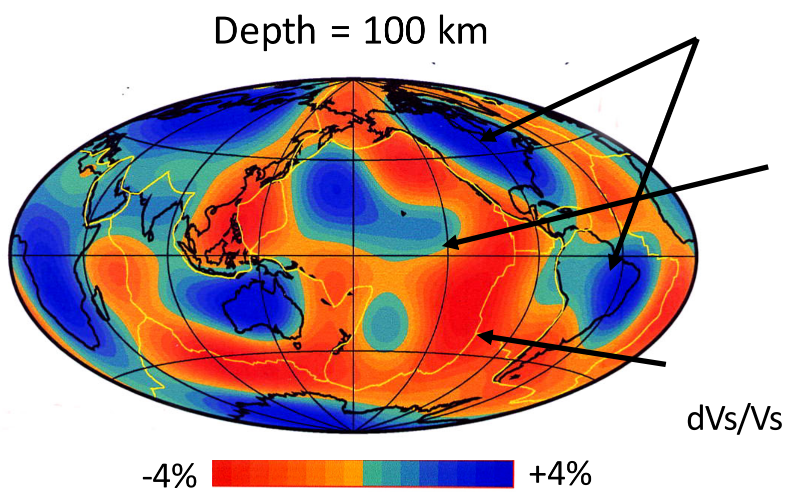

First global 3D model constructed by surface waveform inversion

1977-1984

Model L02.56 (Vp)
Depth = 2500 km

Dziewonski, 1984

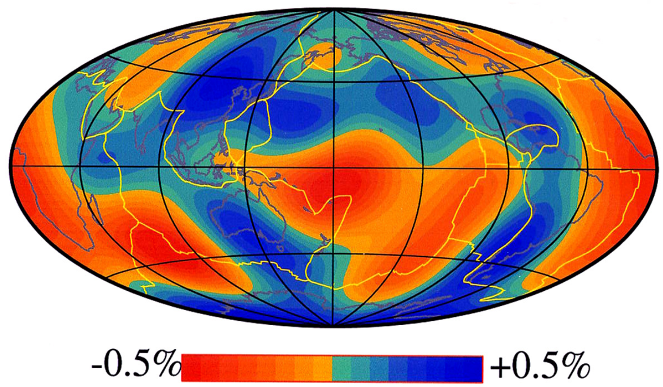

Observed Geoid

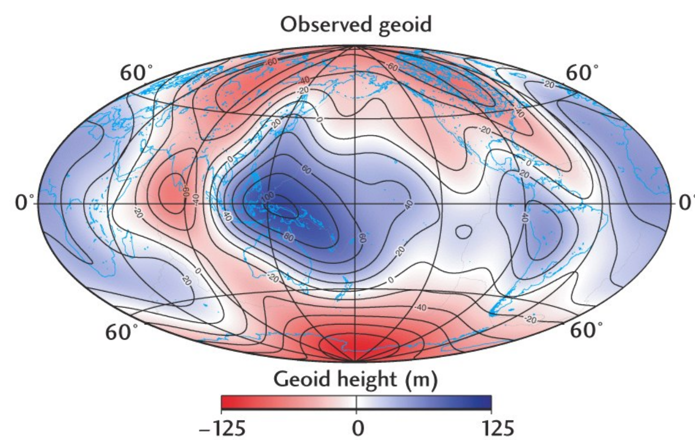

Dziewonski, Hager and O'Connell, 1977

Tectonic reconstructions based on identifying ancient oceanic lithosphere currently located in the lower mantle

Tomographic model
UU-P07
Amaru et al.., 2008
(Utrecht)

Tectonic
reconstructions with
longitude correction
(~ 18 - 20^{o} around
150Ma

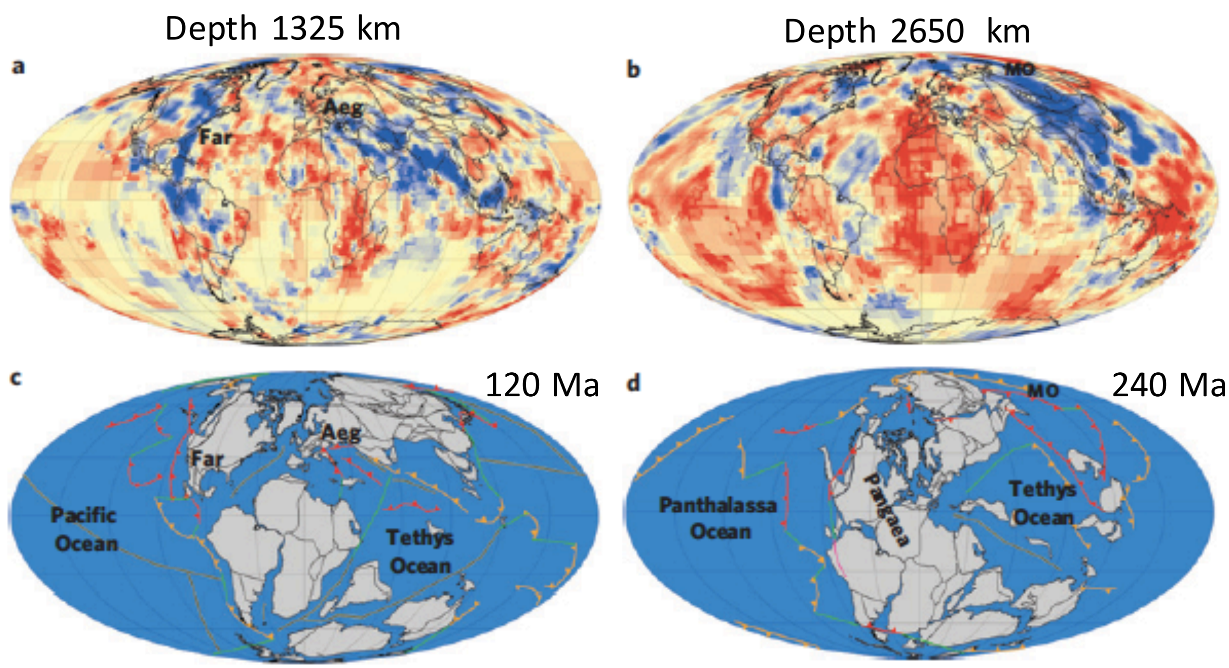

Van der Meer et al., NatGeo, 2010

Principalement:
Ondes de surface
et harmoniques

Depth = 100 km

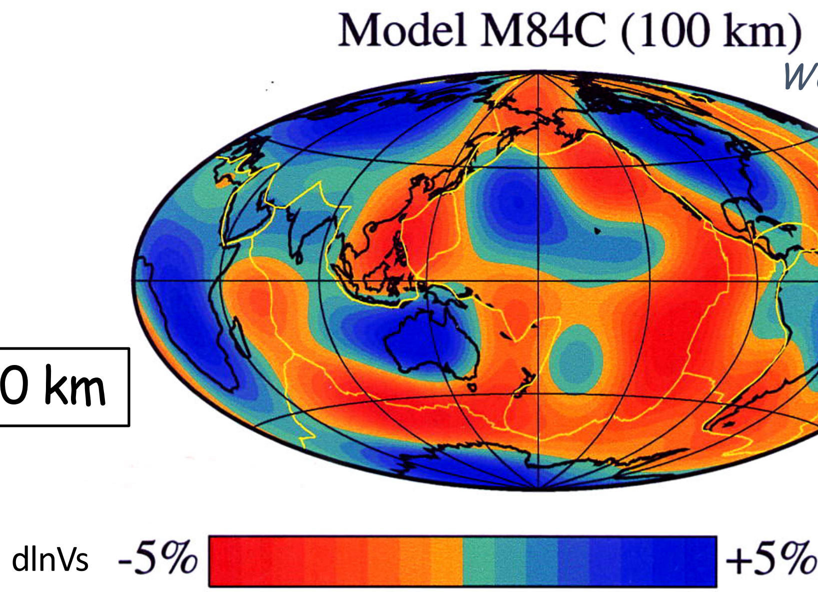

Woodhouse and Dziewonski, 1984

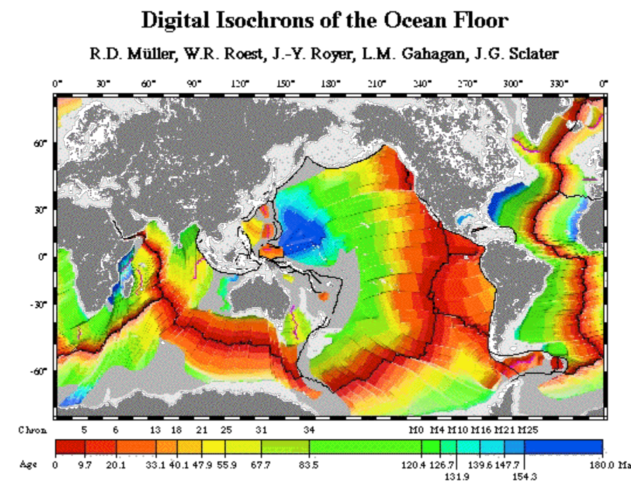

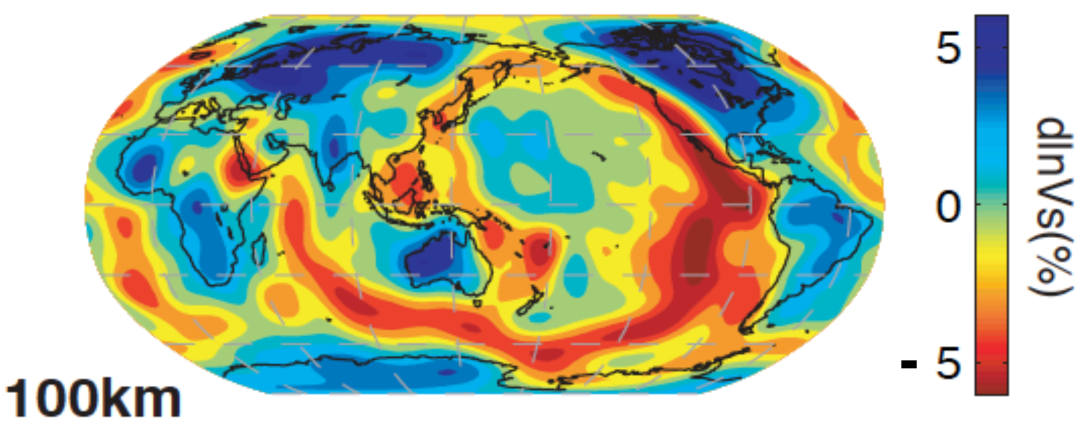

Kustowski et al., 2008

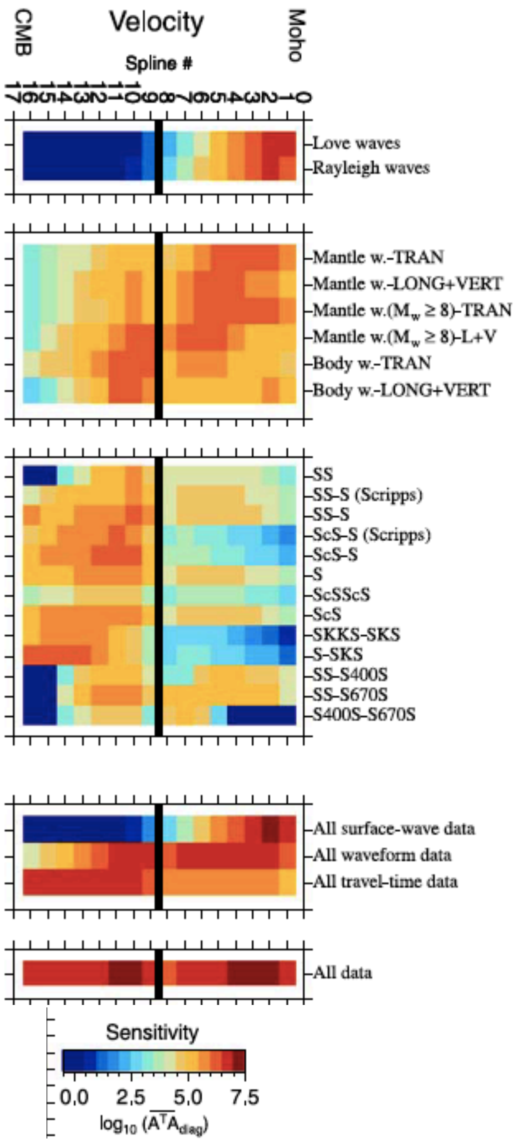

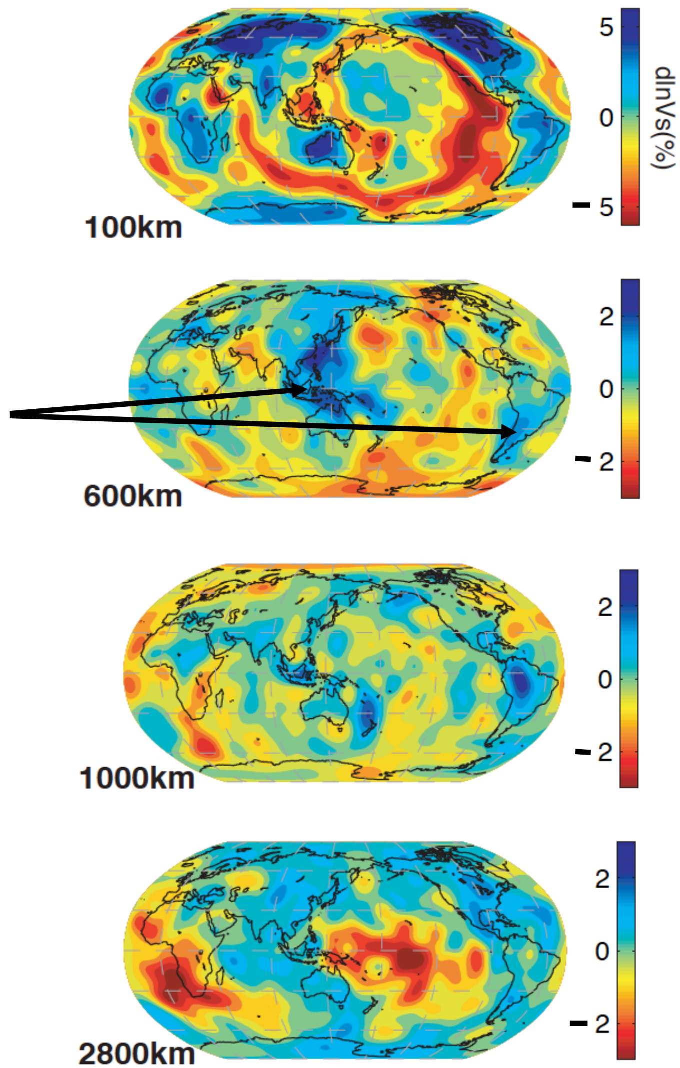

Spectrum of heterogeneity

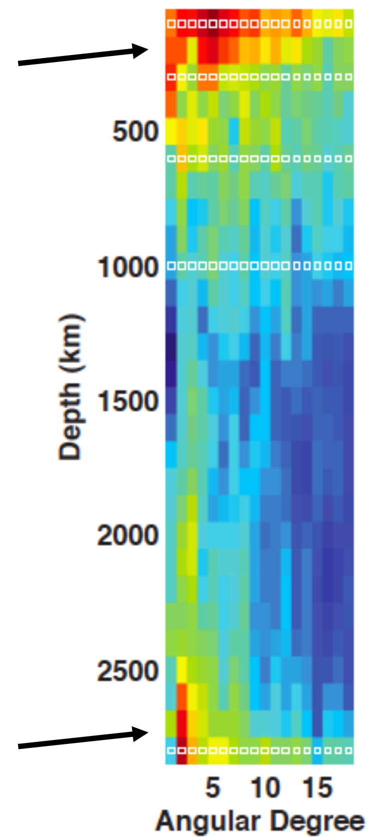

Kustowski et al., 2008